The Roles of Coenzyme A in the Pyruvate:Ferredoxin Oxidoreductase Reaction Mechanism: Rate Enhancement of Electron Transfer from a Radical Intermediate to an Iron−Sulfur Cluster†

Cristina Furdui and Stephen W. Ragsdale*

Department of Biochemistry, Beadle Center, University of Nebraska−Lincoln, Lincoln, Nebraska 68588-0664

Received March 3, 2002; Revised Manuscript Received June 10, 2002

ABSTRACT: Pyruvate:ferredoxin oxidoreductase (PFOR) catalyzes the coenzyme A (CoA)-dependent oxidative decarboxylation of pyruvate. In many autotrophic anaerobes, PFOR links the Wood−Ljungdahl pathway to glycolysis and to cell carbon synthesis. Herein, we cloned and sequenced the *M. thermoacetica* PFOR, demonstrating strong structural homology with the structurally characterized *D. africanus* PFOR, including the presence of three [4Fe-4S] clusters per monomeric unit. The PFOR reaction includes a hydroxyethyl-thiamin pyrophosphate (HE-TPP) radical intermediate, which forms rapidly after PFOR reacts with pyruvate. This step precedes electron transfer from the HE-TPP radical intermediate to an intramolecular [4Fe-4S] cluster. We show that CoA increases the rate of this redox reaction by 10^5-fold. Analysis by Marcus theory indicates that, in the absence of CoA, this is a true electron-transfer reaction; however, in its presence, electron transfer is gated by an adiabatic event. Analysis by the Eyring equation indicates that entropic effects dominate this rate enhancement. Our results indicate that the energy of binding CoA contributes minimally to the rate increase since the thiol group of CoA lends over 40 kJ/mol to the reaction, whereas components of CoA that afford most of the cofactor's binding energy contribute minimally. Major conformational changes also do not appear to explain the rate enhancement. We propose several ways that CoA can accomplish this rate increase, including formation of a highly reducing adduct with the HE-TPP radical to increase the driving force for electron transfer. We also consider the possibility that CoA itself forms part of the electron-transfer pathway.

Pyruvate:ferredoxin oxidoreductase (PFOR)[1] is a thiamin pyrophosphate (TPP), iron−sulfur enzyme that catalyzes the two-electron oxidation of pyruvate to acetyl-CoA (eq 1):

$$CH_3COCOO^- + CoA \leftrightarrow \text{acetyl-CoA} + CO_2 + 2H^+ + 2e^- \quad (1)$$

In the anaerobic bacterium *Moorella thermoacetica* (*f. Clostridium thermoaceticum*), PFOR links glycolysis to the autotrophic Wood−Ljungdahl pathway. In *M. thermoacetica* and some other organisms, PFOR also functions as an efficient pyruvate synthase by a reversal of this reaction (*1*−*3*). The 2.3 Å resolution crystal structure of the *Desulfovibrio africanus* PFOR reveals that the active site cofactor thiamin pyrophosphate (TPP) and a proximal $[Fe_4S_4]^{2+/1+}$ cluster (designated Cluster A) are buried within the protein and that two additional $[Fe_4S_4]^{2+/1+}$ clusters (Cluster B and Cluster C) lead toward the surface, where interactions with a redox partner such as ferredoxin can occur (*4*). Each of the three clusters is separated by ∼13 Å (center-to-center).

Studies of the kinetic mechanism of the *M. thermoacetica* PFOR reveal several interesting features, including a substrate-derived radical intermediate and several long-distance electron-transfer reactions (Figure 1) (*5*). The reaction begins with transient deprotonation of TPP, followed by nucleophilic attack by the resulting TPP carbanion on pyruvate to yield a hydroxyethyl-TPP (HE-TPP) anion or enamine intermediate and CO_2. Next, one electron is transferred from HE-TPP to one of the oxidized $[Fe_4S_4]^{2+/1+}$ clusters (designated Cluster A), which generates a HE-TPP radical intermediate and a reduced $[Fe_4S_4]^{1+}$ cluster. A high-resolution crystal structure of this radical intermediate in the active site of PFOR reveals that the thiazolium ring of the TPP cofactor is markedly bent, indicating loss of aromaticity of the ring (*6*). The next step may involve reaction between the HE-TPP radical intermediate with a sulfur-based CoA radical to generate acetyl-CoA. Alternatively, an electron is transferred from the HE-TPP radical to another Fe-S cluster (Cluster B), to generate a second reduced $[Fe_4S_4]^{1+}$ cluster and the equivalent of an acetyl-TPP intermediate, which undergoes nucleophilic attack by CoA to generate acetyl-CoA. This cluster-to-cluster electron transfer over a 13 Å distance occurs extremely rapidly in the presence of CoA; however, in its absence, the electron-transfer rate, as shown herein, is 100 000-fold

† This work was supported by NIH Grant GM39451 (to S.W.R.).

* Correspondence should be addressed to this author at the Department of Biochemistry, Beadle Center, University of Nebraska−Lincoln, Lincoln, NE 68588-0664. Phone: 402-472-2943; Fax: 402-472-7842; Email: sragsdale1@unl.edu.

[1] Abbreviations: PFOR, pyruvate:ferredoxin oxidoreductase; TPP, thiamin pyrophosphate; CoA, coenzyme A; MOPS, 3-(*N*-morpholino)-propanesulfonate; MV, methyl viologen; acetyl-CoA, acetyl-coenzyme A; desulfo-CoA, desulfo-coenzyme A; 3′-dephospho-CoA, 3′-dephospho-coenzyme A; DTT, dithiothreitol; EPR, electron paramagnetic resonance; RFQ-EPR, rapid freeze−quench EPR.

10.1021/bi0257641 CCC: $22.00
Published on Web 07/12/2002

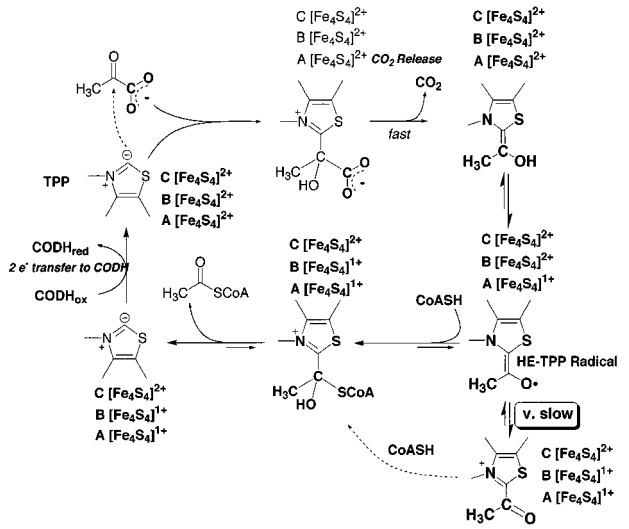

FIGURE 1: Long-distance electron-transfer reactions in PFOR.

slower. Regardless of the presence or absence of CoA, the rate of HE-TPP radical decay matches the rate of $[Fe_4S_4]^{2+/1+}$ cluster reduction; thus, this is a tightly coupled reaction.

In this paper, we have focused on several important questions related to the stability of this radical intermediate. What is the origin of this 10^5-fold rate enhancement for electron transfer from the HE-TPP radical to Cluster B? What is the electron-transfer pathway in the presence versus the absence of CoA? What controls the rate of electron transfer? Does the binding energy of CoA to PFOR contribute to decreasing the energetic barrier of the electron transfer? Is the thiol group of CoA part of the network involved in electron transfer?

To better understand this electron-transfer reaction and the origin of the rate enhancement, we analyzed the rate of electron transfer from the HE-TPP radical intermediate to Cluster B from both transition-state and electron-transfer theory perspectives. We studied the reaction in the presence and absence of CoA and with different CoA analogues to dissect the contributions of different components of the CoA molecule to the electron-transfer rate.

MATERIALS AND METHODS

Materials. N_2 (99.8%, from Linweld) was deoxygenated by passage through a heated column containing BASF catalyst. Pyruvate, CoA, methyl viologen (MV), thiamin diphosphate (TPP), magnesium chloride ($MgCl_2$), 3′-dephospho-CoA, and dithiothreitol (DTT) were purchased from SIGMA. The DIG-High Prime DNA Labeling and Detection Starter Kit II was purchased from Roche Molecular Biochemicals; Taq polymerase, Taq extender, *E. coli* JM 109 competent cells, and the pBluescript KS+ plasmid were purchased from Stratagene. *Bam*HI, Sau3AI, and calf intestinal alkaline phosphatase (CIAP) were purchased from GibcoBRL, and pCR2.1-TOPO vector was acquired from Invitrogen.

Bacterial Strain and Culture Conditions. Moorella thermoacetica (*f. Clostridium thermoaceticum*) strain ATCC 39073 was grown anaerobically at 55 °C in a 14 L fermentor on glucose and CO_2 as carbon source as described (*7*). *E. coli* JM109 was grown in standard LB media with ampicillin.

Enzyme Purification. PFOR was purified under strictly anaerobic conditions as described (*8*) in anaerobic 50 mM 3-(*N*-morpholino)propanesulfonate (MOPS) buffer at pH 7.5. The oxygen level was maintained below 10 ppm in a Vacuum Atmospheres anaerobic chamber. Protein concentration was determined by the Rose Bengal method (*9*) using bovine serum albumin as standard. PFOR activity was measured as described (*5*) following pyruvate- and CoA-dependent MV reduction.

PFOR Sequencing. One primer was designed based on the PFOR N-terminal amino acid sequence: PKQTLDGNTAAAHVAYAMSEVAAIY (5′-gcngcncaygtngcntaygcnatc-3′). The low-redundancy amino acid sequence used to design the C-terminal reverse primer was found by comparing the primary sequences of PFOR from *Desulfovibrio africanus*, *Clostridium pasteurianum*, *Klebsiella pneumoniae*, and *Rhodospirillum rubrum*. The amino acid sequence WIFGGDGW was back-translated to the degenerate primer 5′-ccanccrtcmccnccraakatcca-3′. The two degenerate primers were used in a PCR reaction. The composition of the PCR reaction was 0.5 μM N-terminal primer, 0.5 μM C-terminal primer, 1 μg of genomic DNA, 0.2 mM dNTP, 1.5 mM $MgCl_2$, 1 unit of Taq polymerase, and 1 μL of Taq extender. The buffer used was the Taq extender buffer. The 3 kb PCR product was cloned in a pCR2.1-TOPO vector. The vector containing the insert was transformed in *E. coli* strain JM109 and stored at −80 °C. The PCR product was also used to generate the probe for colony hybridization.

Chromosomal DNA was extracted from *M. thermoacetica* by the standard phenol−chloroform method and was partially digested with Sau3A I. The digestion products were ligated into a pBluescript KS+ plasmid that had been treated with *Bam*HI and CIAP (calf intestinal alkaline phosphatase). The ligation mixture was transformed into *E. coli* JM 109 competent cells and screened by blue−white color selection on plates containing 80 μg/mL X-Gal, 50 μg/mL ampicillin, and 20 mM IPTG. About 90% of the colonies contained an insert. For colony hybridization and detection, we used the DIG-High Prime DNA Labeling and Detection Starter Kit II (Roche Molecular Biochemicals) and followed the protocol suggested in the product manual. The DIG-labeled probe was generated using the 3 kb PCR product as template. The hybridized DIG-labeled probe was detected with an alkaline phosphatase labeled anti-DIG antibody. The blot was incubated with CSPD (disodium 3-(4-methoxyspiro{1,2-dioxetane-3,2′-(5′-chloro)tricyclo[3.3.1.13,7]decan}-4-yl)phenyl phosphate), and the phosphatase activity was detected by chemiluminescence. By exposing the blot to an X-ray film, we found that 1 colony out of 500 contained the PFOR gene. The colony was picked, and both DNA strands were sequenced. The overlapping sequences were manipulated using VectorNTI Suite 6 software (InforMax, Inc.).

Reduction of the Three [4Fe-4S] Clusters followed by UV−Visible Spectroscopy. Throughout the paper, concentrations of PFOR are expressed in terms of the 120 kDa monomeric unit, although the protein exists as a dimer. For the UV−visible scanning spectroscopy, PFOR was diluted to a final concentration of 18.6 μM in 0.5 mL of 50 mM MOPS, pH 7.6, containing 1 mM TPP and 2 mM $MgCl_2$. Then, the enzyme was sequentially reduced at 25 °C by adding 10 mM pyruvate and then 1 mM CoA. Spectra were recorded immediately and 10 min after each addition. In a separate set of experiments, using the same concentration of PFOR, the spectrum was collected before and after the

enzyme was exposed to air for 2 min.

PFOR Reduction followed by Stopped-Flow. All assays were performed in a reaction mixture containing 50 mM MOPS, pH 7.6, 1 mM TPP, 2 mM $MgCl_2$, and 2 mM DTT. All three sets of experiments described below were performed in single wavelength and rapid scanning modes with an Applied Photophysics stopped-flow instrument. One tonometer contained PFOR while the other contained one of the following: (1) 20 mM pyruvate, (2) 20 mM pyruvate and 2 mM CoA, (3) the same as (2) but in the presence of MV (30 and 80 μM initial concentration for the single wavelength experiment and 50, 100, and 400 μM initial concentration for the rapid scanning experiment). In the single wavelength experiments, the PFOR concentration was 30 μM (initial concentration), and the reduction of Fe−S clusters and MV was monitored at 420 and 604 nm, respectively. For the rapid scanning experiments, the PFOR concentration was 40 μM (initial concentration), and spectra were collected between 340 and 750 nm.

EPR Experiments. In parallel with the rapid freeze−quench EPR (RFQ-EPR) experiments at 4 °C, we prepared two EPR samples: (1) 100 μM with 10 mM pyruvate and (2) 100 μM PFOR with 10 mM pyruvate plus 1 mM CoA. The EPR spectra were collected at 10 K, and the parameters were the following: receiver gain, 5×10^3 for the reaction in the absence of CoA and 10^4 for the reaction in the presence of CoA; modulation frequency, 100 kHz; modulation amplitude, 10.145 G; center field, 3400 G; sweep width, 2000 G; and microwave power, 0.2 mW. The double integrals of the EPR signals were compared to that of a 1.1 mM copper(II) perchlorate standard to determine the number of spins per monomeric unit. The power saturation analysis was performed to ensure that the signals were not saturated under our experimental conditions.

Rapid Freeze−Quench EPR Experiments. This experiment was carried out using a chemical/freeze−quench apparatus (Update Instruments, Madison, WI). We performed the experiments at room temperature (20 °C) and at 4 °C by moving the freeze−quench apparatus in the 4 °C cold room. The temperature of the isopentane bath was maintained between −135 and −144 °C. The syringes were made anaerobic by repeated washing with an anaerobically prepared solution containing 50 mM MOPS, pH 7.6, 1 mM TPP, 2 mM $MgCl_2$, and 2 mM DTT. For the 20 °C experiment, PFOR was diluted to 100 μM in the same buffer and loaded in a syringe. The other syringe contained 20 mM pyruvate and 2 mM CoA in the same buffer. The reaction was quenched at 5, 8, 10, 16, 20, and 100 ms by spraying the sample in a bath of cold isopentane (−144 °C). In another experiment, PFOR (100 μM) was reacted with pyruvate alone (20 mM), and the reaction was quenched after 5 ms. The same experiment was repeated at 4 °C in the cold room. The PFOR concentration before mixing was 0.213 mM, and the reaction was quenched at 3, 5, 8, 20, and 100 ms when PFOR was reacted with pyruvate and at 3, 5, 8, 16, 25, 40, and 50 ms when PFOR was reacted with pyruvate and CoA. The EPR spectra were collected immediately after the quench at 77 K, and the parameters were as follows: receiver gain, 10^4; modulation frequency, 100 kHz; modulation amplitude, 10.145 G; center field, 3400 G; sweep width, 2000 G; and microwave power, 0.4 mW.

Temperature Dependence of the Electron-Transfer Rates. We studied the temperature dependence of Cluster A, B, and C reduction, in the presence of pyruvate, pyruvate plus CoA, and pyruvate plus desulfo-CoA. Reduction of the Fe-S clusters was followed at 420 nm, and, depending on the reduction rate, we used a stopped-flow instrument or an Olis spectrophotometer to follow the decay of absorbance at 420 nm. When both pyruvate and CoA were present, Cluster A and Cluster B reduction was followed between 10 and 30 °C, and Cluster C reduction was followed between 10 and 50 °C in an Applied Photophysics stopped-flow instrument, since the reaction was too fast to accurately follow at higher temperatures. One tonometer contained 4.4 mg/mL PFOR (36 μM, initial) in 50 mM MOPS, pH 7.6, 1 mM TPP, 2 mM $MgCl_2$, and 2 mM DTT. The other tonometer contained 20 mM pyruvate and CoA at concentrations ranging from 8 to 800 μM (initial) in the same MOPS buffer. The data shown represent the average of at least five stopped-flow shots and two different batches of enzyme. In the absence of CoA, the same PFOR concentration was used to determine Cluster A reduction in the presence of pyruvate alone (20 mM initial concentration). The reaction was also followed between 10 and 30 °C by stopped-flow. Since Cluster B reduction is slow when PFOR is reacted with pyruvate alone or with pyruvate plus desulfo-CoA, we used temperatures between 10 and 55 °C, and we followed Cluster B reduction in an Olis spectrophotometer. In these experiments, the concentrations of PFOR, pyruvate, and desulfo-CoA were 19 μM, 10 mM, and 1 mM, respectively.

Temperature Dependence of k_{cat}. For these experiments, we coupled the PFOR reaction to methyl viologen (MV) reduction and followed the increase in absorbance at 604 nm. The reaction mixture contained 2 mM DTT, 10 mM pyruvate, 1 mM TPP, 2 mM $MgCl_2$, and 8 mM MV in 50 mM Tris-HCl, pH 7.6. The anaerobic reaction mixture (1 mL) was flushed for 5 min with N_2 before each assay using a Schlenck line. After incubating the reaction mixture for 5 min at temperatures ranging from 10 to 55 °C, CoA was added in concentrations varying from 1.6 to 325 μM, and the reaction was started by adding 1 or 2 μL of 0.032 mg/mL stock PFOR.

PFOR Reduction in D_2O followed by Stopped-Flow. To determine the solvent deuterium kinetic isotope effect on the PFOR reaction in the stopped-flow instrument, we used the optical detection cell in the 2 mm path length mode. The enzyme was successively incubated and washed with buffer made in D_2O (50 mM MOPS, pD 7.6, 1 mM TPP, 2 mM $MgCl_2$, and 2 mM DTT). The solution contained 99% D_2O. PFOR (0.104 mM) was loaded in one tonometer, and the other tonometer contained 20 mM pyruvate and 2 mM CoA in the same buffer. A parallel experiment was performed in H_2O under the same conditions, with 0.22 mM enzyme in one tonometer.

Determination of the Dissociation Constants for Desulfo-CoA and Dephospho-CoA. The K_D (K_I, since it is a competitive inhibitor) for desulfo-CoA was determined at 25 °C in a 0.5 mL reaction mixture containing 2 mM DTT, 10 mM pyruvate, 1 mM TPP, 2 mM $MgCl_2$, and 8 mM MV in 50 mM Tris-HCl, pH 7.6. The desulfo-CoA concentration was varied between 0 and 10 mM at CoA concentrations below, at, and above its K_D (4, 10, and 100 μM). After starting the reaction with 2.2 μg of PFOR, the absorbance

increase at 604 nm due to MV reduction was followed. The kinetic data were fit to a competitive inhibition equation. To measure the effect of desulfo-CoA on the rate of electron transfer from the HE-TPP radical intermediate to Cluster B, we followed the bleaching of the 420 nm band due to cluster reduction. The 0.5 mL reaction mixture contained 19 μM PFOR in 50 mM MOPS buffer, pH 7.5, 1 mM TPP, 2 mM $MgCl_2$, and 2 mM DTT in the presence or absence of 1 mM desulfo-CoA. The reaction was started by adding 10 mM pyruvate and followed at 25 °C. The data were fit to a double exponential decay equation. The K_D for 3′-dephospho-CoA was estimated by single turnover and steady-state kinetic experiments. For the steady-state experiments, the 0.5 mL reaction mixture contained 2 mM DTT, 10 mM pyruvate, 1 mM TPP, 2 mM $MgCl_2$, and 8 mM MV in 50 mM Tris-HCl, pH 7.5. The concentration of 3′-dephospho-CoA was varied between 0.01 and 2 mM. The reaction was performed at 25 °C and was initiated by adding PFOR. The data were fit to the Michaelis−Menten equation to obtain the K_m. In the single turnover experiment, the decrease in absorbance at 420 nm was followed in a stopped-flow experiment. One tonometer contained 94 μM PFOR in 50 mM MOPS buffer, pH 7.6, 1 mM TPP, 2 mM $MgCl_2$, and 2 mM DTT. The other tonometer contained 20 mM pyruvate and five different concentrations of 3′-dephospho-CoA in the same MOPS buffer. The reaction was followed at 25 °C, and the data were fit to a double exponential equation.

Data Analysis. (A) Inhibition Experiments. The $\Delta\Delta G$ for binding was estimated from the K_D values of CoA and CoA analogues (eq 2):

$$\Delta\Delta G_{binding} = -RT \ln(K_{CoA}/K_{analogue}) \quad (2)$$

$\Delta\Delta G$(catalytic) for Cluster C was estimated from the rate constants for MV reduction in the presence of CoA, 3′-dephospho-CoA, or desulfo-CoA and from the rate of Cluster B reduction under the same conditions estimated from pre-steady-state experiments.

(B) Temperature Dependence Experiments. The data were first analyzed by electron-transfer theory using the Marcus equation (eqs 3 and 4):

$$k_{obs} = \frac{4\pi^2 (H_{AB})^2}{h\sqrt{4\pi\lambda RT}} e^{[-(\Delta G'^0+\lambda)^2]/4\lambda RT} \quad (3)$$

$$k_{obs} = k_0 e^{-\beta(r-r_0)} e^{[-(\Delta G'^0+\lambda)^2]/4\lambda RT} \quad (4)$$

The constants in the first two equations are Planck's constant ($h = 6.62608 \times 10^{-34}$ J s), the gas constant ($R = 8.31451$ J K^{-1} mol^{-1}), the characteristic frequency of the nuclei ($k_0 = 10^{13}$ s^{-1}), and the close contact distance of the electron donor and electron acceptor centers ($r_0 = 3$ Å) (*10*, *11*). H_{AB} is the parameter that describes the electronic coupling between the electron donor and the electron acceptor. Its dependence on the distance between the electron donor and the electron acceptor (r, Å) and the nature of the intervening medium (β, $Å^{-1}$) is described in eq 4 (*10*, *12*, *13*). $\Delta G'^0$ is the intrinsic driving force for the electron transfer and is determined by the difference in the midpoint redox potential of the electron donor and the electron acceptor, assuming that the difference between the redox potentials ($\Delta E'^0$ values) for the Cluster A/Cluster B and Cluster B/Cluster C reactions is −25 and −125 mV, respectively. λ is the reorganizational energy, T is the temperature (K), and k_{obs} is the observed rate of electron transfer (s^{-1}) (*10*). By fitting the observed rate constant for electron transfer as a function of temperature to eq 3, $\Delta G'^0$, H_{AB}, and λ can be determined. The values of $\Delta G'^0$ and λ are then used in eq 4, to estimate β and r.

When the parameters estimated by ET theory showed that the reaction is not a true electron transfer, we used transition-state theory to determine the activation parameters ($\Delta H^{\ddagger}$, $\Delta S^{\ddagger}$) for the process that gates the electron-transfer reaction. We used a nonlinear, least-squares fit of the data to the Eyring equation (eq 5):

$$k_{obs} = \frac{k_B T}{h} e^{-(\Delta H^{\ddagger}/RT + \Delta S^{\ddagger}/R)} \quad (5)$$

The constants in eq 5 are Planck's constant (h), the gas constant (R), and Boltzmann's constant (k_B, 1.38066×10^{-23} J K^{-1}).

Kinetic Simulation. Kinetic simulations of the mechanism were performed based on the single wavelength stopped-flow data (described above under *PFOR Reduction followed by Stopped-Flow*) and based on the RFQ-EPR data at 4 °C for the formation and decay of the HE-TPP radical intermediate. The proposed mechanism and the results are described under Results and in Scheme 1. The simulations were performed using Kinsim: Chemical Kinetic Simulation System (*14*, *15*). To simulate the change in absorbance at 420 and 604 nm, and the formation and the decay of the HE-TPP radical intermediate, we used the following output equations:

$$A_{420} = 19.7*(D + DA) + 15*(EA + EAB) + 12.4*(FC + FD + F + FA + G) + 7.5*(J + K) + 2.6*(L + LO) + 2.2*M + 10.1*H + 0.32$$

$$A_{604nm} = 13.9*M + 0.164$$

Then, to simulate radical formation and decay, we used this equation: $I = (8 \times 10^5)*(EA + EAB) + (8 \times 10^5)*(J + K)$. In these equations, *D*, *DA*, *EA*, *EAB*, *FC*, *FD*, *F*, *FA*, *G*, *J*, *K*, *L*, *LO*, *M*, and *H* are the concentrations of the reactants and intermediates in the mechanism described in Scheme 1, and 19.7, 16.4, 12.4, 7.5, 2.6, and 10.1 are the extinction coefficients at 420 nm of the different species in Scheme 1, using 7.5 mM^{-1} cm^{-1} as the extinction coefficient for one oxidized cluster. We estimated the extinction coefficient of MV at 420 nm, 2.2 mM^{-1} cm^{-1}, by reducing MV with dithionite and calculating the MV concentration from the absorbance at 604 nm ($\epsilon = 13.9$ mM^{-1} cm^{-1}) (data not shown). 0.32 OD is the absorbance at 420 nm of the fully reduced enzyme. The initial concentrations of PFOR, pyruvate, CoA, and MV for the three reactions (PFOR and pyruvate, PFOR and pyruvate plus CoA, and PFOR and pyruvate plus CoA in the presence of MV) were as follows: PFOR, 0.015 mM; pyruvate, 10 mM; CoA, 1 mM; MV, 0.016 mM. To simulate the reaction with pyruvate alone, the concentrations of CoA and MV were set to zero, since these were not present in the reaction, and this stops the simulation at step 2. We followed, therefore, the formation of the radical intermediate and the reduction of Cluster A. To simulate the reaction of PFOR with pyruvate and CoA,

Scheme 1

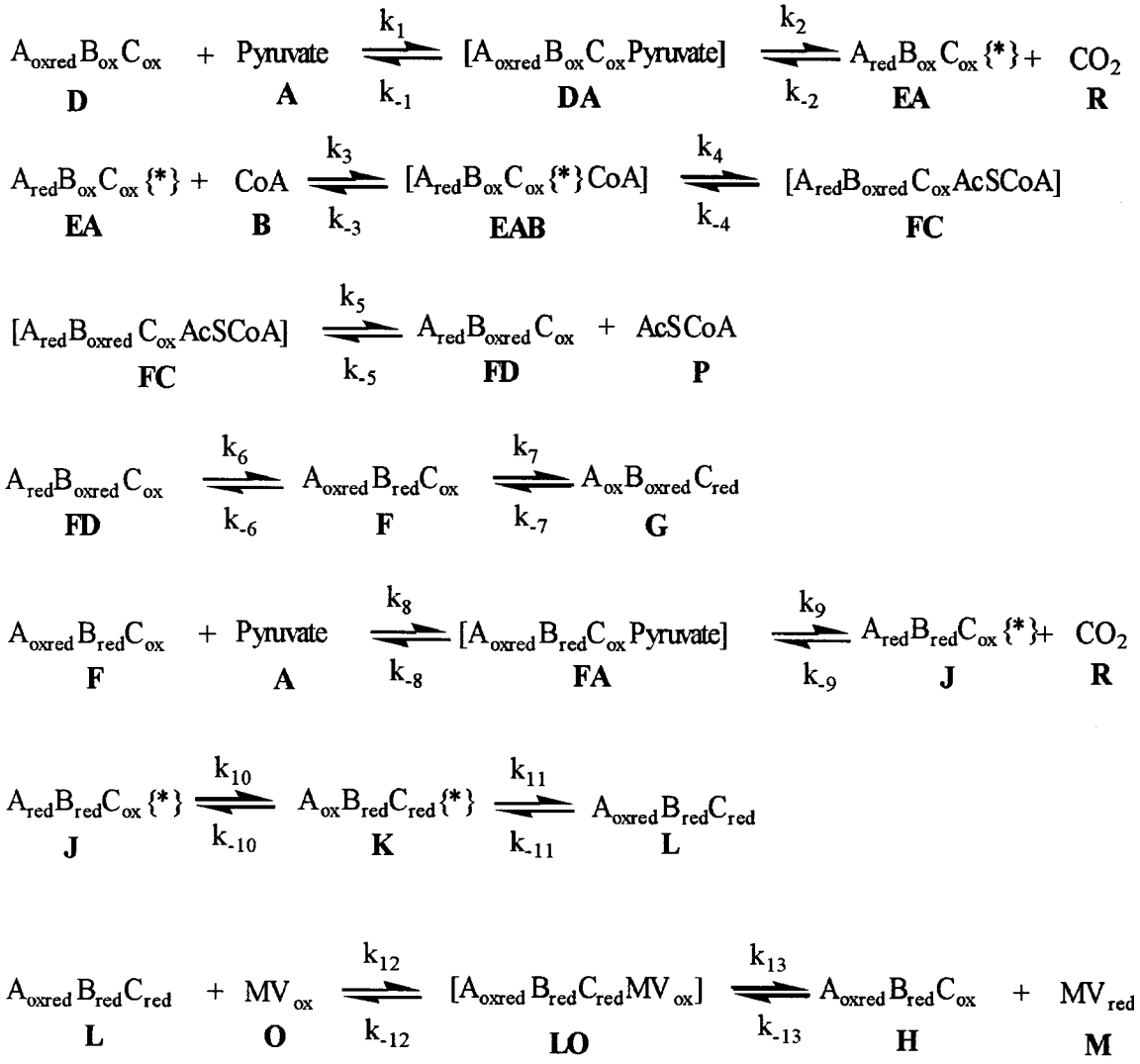

we set MV concentration to zero which stops the reaction at step 11. This allowed us to follow Cluster A and Cluster B reduction, electron transfer between clusters, and the second turnover of the enzyme to result in an 86% reduced enzyme. These conditions were also used to simulate the formation and the decay of the HE-TPP radical intermediate. For the reaction in the presence of MV, we added two more steps (reactions 12 and 13) which describe the electron transfer from Cluster C to MV. As can be seen in the mechanism, two other species, G and K, have Cluster C reduced and theoretically could donate one electron to MV. However, we chose to include only L because G and K accumulate to very low amounts relative to L.

RESULTS

Sequence and Cluster Composition

Nomenclature. The *Desulfovibrio africanus* PFOR contains three [4Fe-4S] clusters that have been defined as the proximal, medial, and distal clusters on the basis of their structurally determined distance from the TPP cofactor (*4*). Here, we designate them as Clusters A, B, and C on the basis of their reduction rates, with Cluster A being reduced at the fastest rate and Cluster C, the slowest. The relationship between the kinetic- and the structure-based nomenclature is discussed below.

Sequence of the M. thermoacetica PFOR. We cloned and sequenced the *M. thermoacetica* PFOR and found that the enzyme shares 59% sequence identity with the *D. africanus* enzyme, whose structure is known (*4*). The two proteins share six domains (Figure 2), but the *D. africanus* PFOR contains an additional C-terminal domain that is lacking in the *M. thermoacetica* protein and is proposed to protect it against oxygen damage (*4*). Domains I, III, and VI are involved in binding TPP. Within Domain VI, the most extensive interactions are H-bond contacts between the oxygen atoms of the pyrophosphate and amino acid residues T965 (amide N), S995 (amide N), E817 (carboxyl O), C840 (amide N), and N996 (N) and two water molecules. The amino acid numbering is based on the *D. africanus* sequence. Conserved residue N996 also forms a hydrogen bond interaction with the thiazole sulfur of TPP. F869 stacks against the thiazolium ring and is in the position of I415 in pyruvate decarboxylase, which promotes formation of the V-conformation between the pyrimidine and thiazolium ring (*16*). Also within Domain VI, cysteine residues 812, 815, 840, and 1071, which ligate the proximal [4Fe-4S] cluster, are conserved. Domain V is an 8 Fe ferredoxin-like domain

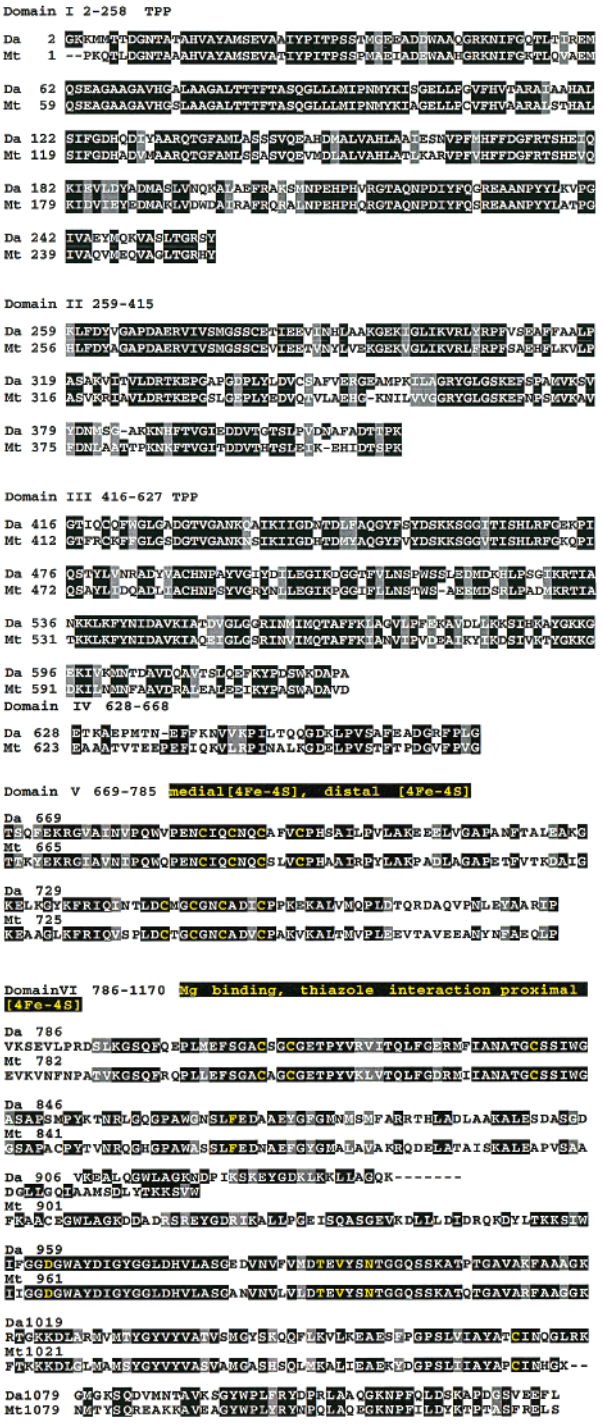

FIGURE 2: Structural homology between the *M. thermoacetica* and *D. africanus* PFORs. (A) Domain arrangement and sequence homology. (B) Relative positions of the redox centers in PFOR [derived from (*4*)].

containing the 8 cysteine residues required for binding the medial and distal [4Fe-4S] clusters. Based again on the strong homology between the *D. africanus* and *M. thermoacetica* enzymes, conserved cysteine residues 689, 692, 695, and 755 can be assigned as the ligands for Distal Cluster C and conserved residues 745, 748, 751, and 699 as the ligands for Medial Cluster B. These results strongly indicate that the *M. thermoacetica* enzyme possesses three [4Fe-4S] clusters per monomeric unit as suggested earlier based on evolutionary considerations (*4*), and in contrast to earlier conclusions (*5*, *17*). The high level of sequence homology

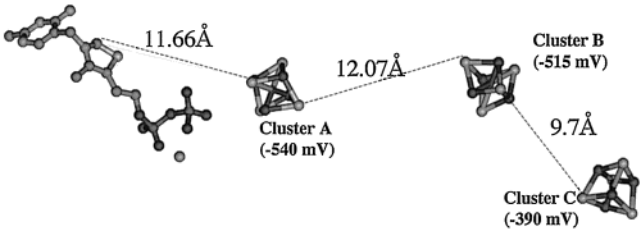

FIGURE 3: Spatial organization of the three [4Fe-4S] clusters in *D. africanus* PFOR. The redox potential for the three clusters is taken from (*4*). The edge-to-edge distance was estimated using Chime software.

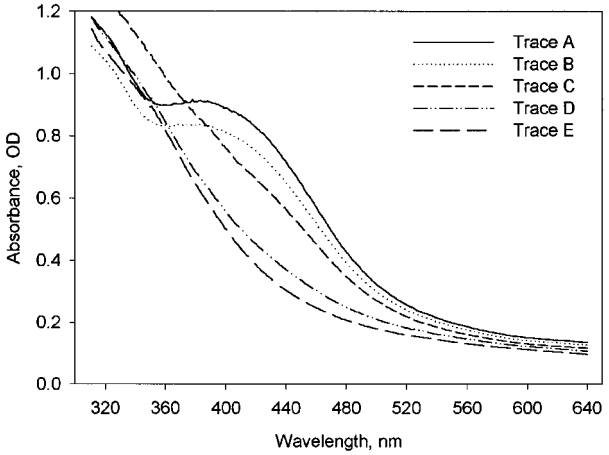

FIGURE 4: UV−visible spectra of PFOR reduction. Spectra of 18.6 μM PFOR were recorded under five conditions. Trace A represents the air-oxidized enzyme, Trace B as-isolated enzyme, Trace C enzyme reduced with 10 mM pyruvate, Trace D enzyme reduced with 10 mM pyruvate and 1 mM CoA, and Trace E represents the enzyme incubated 10 min with 10 mM pyruvate and 1 mM CoA when complete reduction of the three clusters is achieved.

strongly indicates that the overall structures of the *M. thermoacetica* and *D. africanus* PFORs are conserved and that the distances between the redox centers are very similar (Figure 3). To explain the previous conclusions that *M. thermoacetica* PFOR contains two $[Fe_4S_4]^{2+/1+}$ (*5*, *17*), it appears that one of the clusters was labile and partially absent. This would also explain the higher specific activity and the faster kinetic constants measured than the enzyme studied over the past several years.

Metal Content and Spectroscopic Studies of M. thermoacetica PFOR. In this paper, we reinvestigated the iron content and the UV−visible spectroscopic properties and related these measurements to a protein concentration determined by dry weight and amino acid analysis. Considering an extinction coefficient at 400 nm of 48 000 M^{-1} cm^{-1} (*18*), the average cluster stoichiometry per monomeric unit of enzyme (120 kDa) is 3.0 ± 0.1 [4Fe-4S] clusters. The same number of [4Fe-4S] clusters/monomer PFOR is obtained if we measure the difference spectrum at 420 nm between oxidized and pyruvate-plus-CoA reduced enzyme, assuming a $\Delta\epsilon_{ox-red}$ at 420 nm of 7500 M^{-1} cm^{-1} for one cluster (Figure 4). When the UV−visible spectrum of the as-isolated enzyme (Trace B) is compared with that after 2 min exposure to air (Trace A), it is clear that 0.4 cluster in the as-isolated enzyme is partially reduced, assuming a $\Delta\epsilon_{ox-red}$ of 7500 M^{-1} cm^{-1}, leaving 2.6 clusters in the oxidized 2+ state. Addition of 10 mM pyruvate to the as-isolated enzyme (Trace C) apparently reduces the remainder

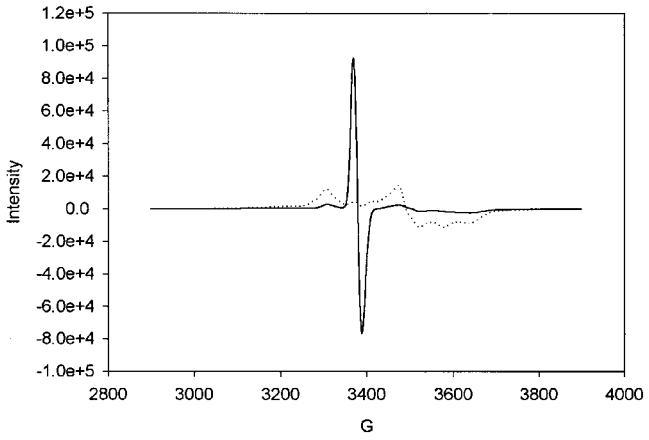

FIGURE 5: EPR spectroscopy. 100 μM PFOR was reduced with 10 mM pyruvate (solid line, 0.4 spin of HE-TPP radical/monomer, 1.5 total spins/monomer) and with 10 mM pyruvate and 1 mM CoA (dashed line, 2.6 total spins/monomer). The parameters were: receiver gain 5×10^3 (solid line) and 10^4 (dashed line), modulation frequency 100 kHz, modulation amplitude 10.145 G, center field 3400 G, sweep width 2000 G, and microwave power 0.2 mW, 10 K.

of this cluster, yielding a total of 1.0 cluster in the 1+ state. A second cluster slowly (over 5−20 min) undergoes reduction, whereas addition of 10 mM pyruvate and 1 mM CoA (Traces D and E) quickly reduces all three clusters to the 1+ state. Thus, the difference spectrum at 420 nm between Trace A and Trace E gives a $\Delta\epsilon$ of 22.5 mM^{-1} cm^{-1}, corresponding to three [4Fe-4S] clusters being reduced.

The UV−visible results were confirmed by EPR spectra. We recorded the EPR spectra of the enzyme, as-isolated, enzyme plus pyruvate, and enzyme plus pyruvate and CoA. Generally, when the as-isolated enzyme is reacted with pyruvate alone, the amount of HE-TPP radical intermediate varies from 0.4 to 0.6 spin per monomeric unit. The EPR signal intensity of the HE-TPP radical formed upon reaction with pyruvate appears to correlate with the amount of oxidized Cluster A present in the as-isolated protein. The as-isolated enzyme exhibits the characteristic EPR spectrum of a $[4Fe\text{-}4S]^{1+}$ cluster with a spin integration of 0.4 spin/monomer (spectrum not shown). The EPR signal in Trace A integrates to 1.5 total spins/monomer. The $g = 2.0$ signal contributes 0.4 spin/monomer, which correlates with the amount of available oxidized Cluster A based on the stopped-flow experiments, EPR analysis of the as-isolated protein, and UV−visible experiments (Figure 5, solid line). When the enzyme is treated with pyruvate plus CoA (1 min incubation at 20 °C) (Figure 5, dashed line), the EPR spectrum is complex, and the signal integration yields 2.6 spins/monomer. In summary, DNA sequence analysis, UV−visible spectroscopy, and EPR spectroscopy concur that the *M. thermoacetica* PFOR contains three $[4Fe\text{-}4S]^{2+/1+}$ clusters. The high degree of homology with the *D. africanus* enzyme strongly suggests that they are located in the same positions as those of the *D. africanus* enzyme (*4*). Therefore, we feel justified to use the *D. africanus* structure as a model to help interpret the electron-transfer steps in the *M. thermoacetica* enzyme.

Kinetic Studies

We have performed pre-steady-state and steady-state kinetic experiments in the presence and absence of CoA, pyruvate, and electron acceptor (Figure 6) to follow the internal electron-transfer reactions among the component redox centers, the three FeS clusters (A, B, and C), and HE-TPP. The optimum temperature for the PFOR reaction is 55 °C; however, because the electron-transfer rates are much too fast to monitor at this temperature, we performed most of these studies at 10 °C. We used as-isolated enzyme, in which Cluster A is partially reduced by the DTT in the buffer (see above). Omitting the reductant results in enzyme inactivation. The dashed line in Figure 6 represents the Kinsim simulation of the mechanism described by Scheme 1. In this mechanism, A, B, and C designate Cluster A, Cluster B, and Cluster C and the asterisk (*) designates the HE-TPP radical intermediate. The same kinetic scheme (Scheme 1) was used to fit all the data; however, the

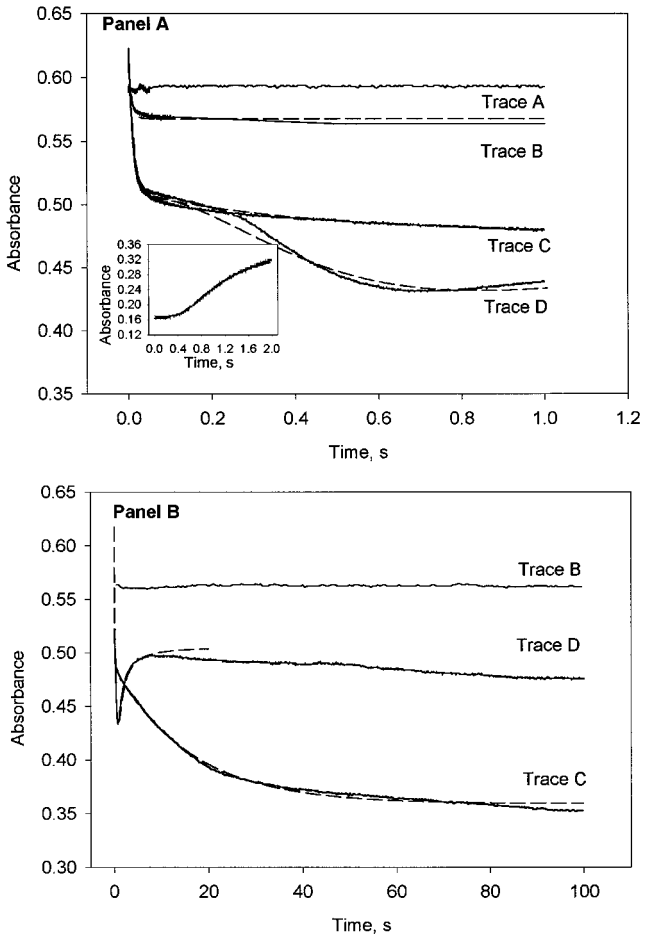

FIGURE 6: PFOR reduction followed by stopped-flow. Panel A: 1 s time scale of the reaction. Panel B: the 100 s time scale of the reaction. In both panels, Trace A represents the initial absorbance of the as-isolated enzyme at 420 nm (the starting absorbance is indicated by the arrow), Trace B represents the change in absorbance at 420 nm due to the reduction of PFOR ($A_1 = 0.038$ OD, $k_1 = 140$ s^{-1}) with 10 mM pyruvate in the absence of CoA, Trace C follows the reduction of PFOR in the presence of 10 mM pyruvate and 1 mM CoA ($A_1 = 0.038$ OD, $k_1 = 140$ s^{-1}; $A_2 = 0.038$ OD, $k_2 = 140$ s^{-1}; $A_3 = 0.038$ OD, $k_3 = 4.7$ s^{-1}), and Trace D follows the reduction of PFOR with 10 mM pyruvate, 1 mM CoA, and 15 μM MV ($A_1 = 0.038$ OD, $k_1 = 140$ s^{-1}; $A_2 = 0.038$ OD, $k_2 = 140$ s^{-1}; $A_3 = 0.03$ OD, $k_3 = 4.7$ s^{-1}; $A_4 = 0.07$, $k_4 = 5$). The expected absorbance of the fully oxidized enzyme is 0.67 OD, and the expected change in OD for the reduction of one cluster is 0.11 OD. In the inset of Panel A we followed the reduction of 0.016 mM MV at 604 nm under the same conditions as Trace D ($A = 0.216$, $k = 0.74$ s^{-1}, OD/s = 0.12).

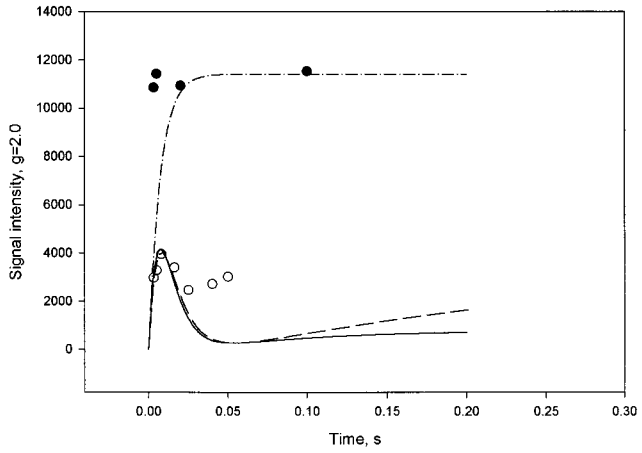

FIGURE 7: RFQ-EPR at 4 °C. A solution containing PFOR (200 μM) was reacted with an equal volume of solution containing 20 mM pyruvate (●) or pyruvate plus 2 mM CoA (○). The intensity of the $g = 2.0$ signal from the HE-TPP radical was monitored by EPR spectroscopy at 77 K. The lines represent the Kinsim simulation of the formation and the decay of the HE-TPP radical intermediate according to the proposed mechanism. The dashed−dotted line is the result of Kinsim simulation using the parameters in column 1, Table 1, the dashed line was obtained using the parameters in column 2a, and the solid line was obtained using the parameters in column 2b, Table 1.

mechanism was truncated when appropriate by setting the concentration of reagents to zero. For example, when PFOR was reacted with pyruvate only, we used the full kinetic scheme, but we set the CoA and MV concentrations to zero, which effectively truncates the mechanism at step 2.

PFOR Reaction with Pyruvate. When the as-isolated enzyme is reacted with buffer alone, the initial absorbance at 420 nm is 0.59 (Figure 6, Panel A, Trace A). The absorbance of the air-oxidized enzyme is 0.67. The expected absorbance change for the reduction of one cluster is 0.115. Thus, Cluster A in the as-isolated enzyme is already 65% reduced [(0.67 − 0.595)/0.115]. We fit the kinetic traces to exponential equations to derive an initial estimate of the electron-transfer rate constants. Then, we used kinetic simulation of the traces to derive a more accurate and self-consistent set of rate constants. When PFOR is reacted with pyruvate alone at 25 °C, the amplitude of the absorption decrease is 0.04, which corresponds to 30% reduction of one [4Fe-4S] cluster (Cluster A) within the 2.3 ms dead time of the stopped-flow instrument. Thus, at 25 °C, its rate constant exceeds 500 s^{-1}. To obtain accurate rate constants, we followed Cluster A reduction at 10 °C, which yields a rate constant of 140 s^{-1} (Panel A, Trace B). The dashed line represents the Kinsim simulation according to Scheme 1 with the following rate constants: $k_1 = 900$ mM^{-1} s^{-1}, $k_{-1} = 200$ s^{-1}, $k_2 = 140$ s^{-1}. Based on these rate constants, we calculate a K_m for pyruvate of 0.3 mM, which is identical to the value measured by steady-state experiments (data not shown).

When PFOR is reacted with pyruvate in the absence of CoA at 4 °C, the maximum amount of the $g = 2.0$ EPR signal characteristic of the HE-TPP radical is 0.35 spin/monomer. Thus, the amount of HE-TPP radical formed when PFOR is reacted with pyruvate equals the amount of available oxidized Cluster A. The maximum amount of the radical observed in the RFQ-EPR experiment is 0.14 spin/monomer. This signal accumulates within 3 ms (Figure 7, filled circles) at a rate that is consistent with the rate of Cluster A reduction (estimated from the stopped-flow experiment, 140 s^{-1}), and decays very slowly over 5−20 min. Therefore, radical formation and Cluster A reduction occur at the same rate. The Kinsim simulation of the RFQ-EPR data for HE-TPP radical formation is presented in the dashed−dotted line in Figure 7. When PFOR and pyruvate are mixed at 25 °C and the reaction is followed by stopped-flow and RFQ-EPR, the results are also consistent and indicate that Cluster A reduction and HE-TPP radical formation occur within 5 ms of mixing. These reactions occur at a rate that is independent of the presence of CoA or external electron acceptor (below) as was observed in earlier studies (*5*). Thus, in the initial stages of the PFOR mechanism, pyruvate forms an adduct with TPP that undergoes decarboxylation and then transfers one electron to Cluster A, forming the HE-TPP radical intermediate.

Following the reduction of Cluster A, Cluster B is reduced (Figure 6, Panel B, Trace B) ($k_{obs} = 0.001$ s^{-1} at 10 °C and 0.003 s^{-1} at 25 °C) at the same slow rate as that of HE-TPP radical decay. This is consistent with earlier studies demonstrating tight coupling between HE-TPP radical decay and Cluster B reduction (*5*).

PFOR Reaction with Pyruvate and CoA. When PFOR reacts with pyruvate at 10 °C, the rate of Cluster A reduction is the same (140 s^{-1}) in the absence or presence of CoA. Then, in the presence of CoA, Cluster B undergoes a partial reduction with a rate constant of 140 s^{-1} and an amplitude of 0.039 that corresponds to the amount of HE-TPP radical formed (Figure 6, Panel A, Trace C). This is 10^5-fold faster than the rate of Cluster B reduction in the absence of CoA. In a parallel RFQ-EPR experiment, when PFOR is reacted with pyruvate plus CoA at 4 °C, the HE-TPP radical intermediate forms and decays at a rate constant consistent with the rate of Cluster A and Cluster B reduction (Figure 7, empty circles). The maximum amplitude of the $g = 2$ EPR signal is approximately 33% of that obtained when the enzyme is reacted with pyruvate alone, indicating that the HE-TPP intermediate forms and is consumed at equal rates. We conclude that, in the presence of pyruvate and CoA, the radical intermediate first forms at a rate equal to that of Cluster A reduction and then decays at a rate equal to that of Cluster B reduction. The Kinsim simulation of the first 100 ms of the reaction includes the first five reaction steps of the mechanism described above (see the dashed lines in Figure 6, Panel A, Trace C, and in Figure 7). The additional rate constants are as follows: $k_3 = 1.1 \times 10^5$ mM^{-1} s^{-1}, $k_{-3} = 200$ s^{-1}, $k_4 = 140$ s^{-1}, $k_{-4} = 0.1$ s^{-1}, $k_5 = 120$ s^{-1}, and $k_{-5} = 0.01$ s^{-1}. When the reaction of PFOR with pyruvate and CoA is followed for a longer time at 10 °C, further and complete reduction of PFOR can be observed with two additional phases of 5 and 0.08 s^{-1} (Figure 6, Panel B, Trace C).

The proposed Kinsim mechanism accounts for the complete reduction of the enzyme in the absence of an external electron acceptor (steps 6 through 11). However, to achieve full reduction of the enzyme, a second mole of pyruvate must bind because pyruvate oxidation is a two-electron process and the enzyme contains three [4Fe-4S] clusters (i.e., which are able to accept as many as three electrons). Based on the *D. africanus* PFOR structure, showing Cluster A near the C-2 of the TPP thiazolium ring, we suggest that before the

Table 1: Rate Constants, Concentrations, and Output Constants Used in Kinsim Analysis

	pyruvate	pyruvate + coenzyme A		pyruvate + CoA + MV
rate constants	1	2a	2b	3
k_1, $mM^{-1}\,s^{-1}$	900	900	900	900
k_{-1}, s^{-1}	200	200	200	200
k_2, s^{-1}	140	140	140	140
k_{-2}, s^{-1}	0.1	0.1	0.1	0.1
k_3, $mM^{-1}\,s^{-1}$		1.1×10^5	1.1×10^5	1.1×10^5
k_{-3}, s^{-1}		200	200	200
k_4, s^{-1}		140	140	140
k_{-4}, s^{-1}		0.1	0.1	0.1
k_{+5}, s^{-1}		120	120	4.00
k_{-5}, s^{-1}		0.1	0.001	0.1
k_{+6}, s^{-1}		40	5	5
k_{-6}, s^{-1}		0.01	0.21	0.21
k_{+7}, s^{-1}		4.6	16000	4.6
k_{-7}, s^{-1}		0.21	0.4	0.21
k_{+8}, $mM^{-1}\,s^{-1}$		92.78	900	900
k_{-8}, s^{-1}		1102	200	200
k_{+9}, s^{-1}		2.3	100	100
k_{-9}, s^{-1}		0.001	0.1	0.1
k_{+10}, s^{-1}		5	5	5
k_{-10}, s^{-1}		0.1	0.1	0.1
k_{+11}, s^{-1}		0.27	120	120
k_{-11}, s^{-1}		0.001	0.01	0.01
k_{+12}, $mM^{-1}\,s^{-1}$				900
k_{-12}, s^{-1}				750
k_{+13}, s^{-1}				120
k_{-13}, s^{-1}				0.1

second mole of pyruvate binds to the enzyme, Cluster A must be oxidized. One or two intramolecular cluster-to-cluster electron-transfer steps (steps 6 and 7) could oxidize Cluster A. Binding of pyruvate to species F can take place with the same affinity and rate as to species D, or, since F has Cluster B reduced, these rates might be different. We could fit Trace C in Figure 6, Panels A and B, and formation and decay of the radical intermediate (Figure 7, open circles) with two very different sets of rate constants (Table 1, columns 2a and 2b) for steps 6 to 11, the rate constants for the first five steps being the same as described above.

While the stopped-flow data are simulated quite well by Scheme 1 and the rate constants in columns 2a and 2b, the RFQ-EPR data shown in Figure 7 for the reaction including pyruvate and CoA are multiexponential and exhibit too much complexity for all the kinetic phases to be accommodated. The formation and decay of the HE-TPP radical, which occurs in the first 30 ms, matches the simulation quite well; however, in the simulation, the radical decays to nearly zero intensity before it again builds up, whereas the intensity of the radical EPR signal remains relatively higher. We also have not shown or attempted to simulate what happens over the next 40 s, where the radical decays to zero. The problem relates to our simplification of an already complex mechanism shown in Scheme 1. There are many possible ways for the HE-TPP radical intermediate to re-form, whereas the mechanism described in Scheme 1 represents only one way. Any of the species that contain oxidized Cluster A (past step 5) can bind a second mole of pyruvate and regenerate the HE-TPP radical. Nevertheless, our major interest is in what is happening in the initial stage of the reaction, and the data and simulations match the formation and decay of the radical quite well during the first 30 ms of the reaction. In the Kinsim mechanism described in Scheme 1, intermediate L has 60%

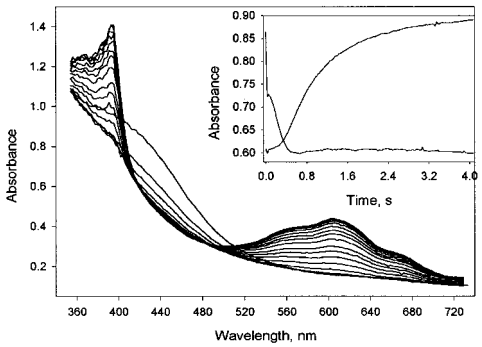

FIGURE 8: PFOR reduction (20 μM monomer final concentration) by 10 mM pyruvate and 1 mM CoA, in the presence of 25 μM MV, followed by rapid scanning spectroscopy at 10 °C. We collected 1600 scans over a time scale of 4 s. Inset: the relative absorbance of MV at 604 nm was overlapped with PFOR reduction at 420 nm. We also used 50 and 200 μM MV in two other rapid scanning experiments at the same concentrations of PFOR, pyruvate, and CoA.

of Cluster A in the reduced state, and Clusters B and C are also reduced. The spin concentration expected for this state is 2.6 spins/monomer, and, for this reason, we attribute the dashed line spectrum in Figure 5 to intermediate L (Scheme 1).

PFOR Reduction by Pyruvate and CoA in the Presence of MV. In the presence of saturating concentrations of an external electron acceptor (e.g., MV), the k_{cat} for the PFOR reaction at 10 °C is 5 s^{-1}. When PFOR is reacted with pyruvate, CoA, and subsaturating levels of MV (16 μM, final concentration), the rates of Cluster A and B reduction remain unchanged; however, the shape of the third phase is complex, indicating a series of reduction and oxidation steps (Figure 6, Panel A, Trace D). The fit to these data is not as good as with the other traces. This is because we chose to include only the intermediate that accumulates in the highest concentration in the reaction with MV (intermediate L). When the other intermediates are included, a better fit to the data can be obtained. There are other intermediates that could donate electrons to MV. When reduction of MV at 604 nm is followed under these conditions (inset of Figure 6, Panel A), we observe a 300 ms lag phase, followed by an absorbance increase at 604 nm occurring with a rate constant of 0.6 s^{-1}. Using the mechanism described by Scheme 1 and the values determined above, we assigned the reduction/oxidation phases to different elementary reaction steps, as presented in Table 1, column 3. Comparing the reaction of PFOR with pyruvate and CoA in the presence versus the absence of MV indicates that MV changes the rate constants of steps 5 and 7 (from Table 1, column 2b) and steps 5, 6, 8, and 9 (Table 1, column 2a). This implies that pyruvate binds to F with the same affinity as it binds to D and that, in the presence of MV, Cluster B reduces Cluster C (steps 7 and 10) at a rate constant of 5 s^{-1}, which equals the k_{cat} for the reaction at the same temperature.

We also followed the reaction of PFOR with pyruvate, CoA, and varying low concentrations of MV by rapid scanning stopped-flow (Figure 8, 25 μM MV). These are *V/K* conditions for MV. By extracting the trace at 420 nm and fitting to an exponential decay equation, we determined the rate constants for Cluster A and B reduction, which agreed with those obtained from the single wavelength experiment. Then, when the absorbance at 604 nm is

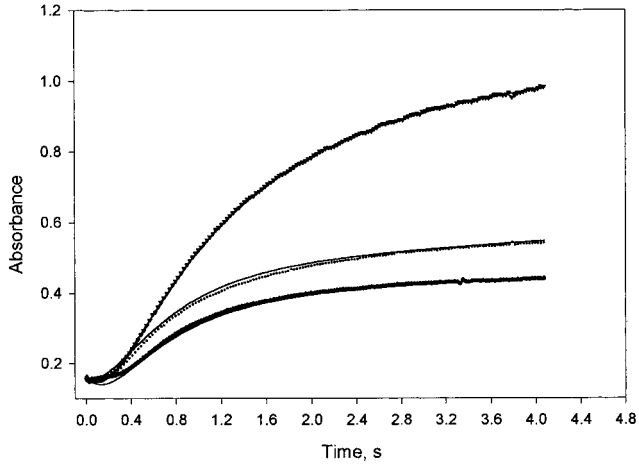

FIGURE 9: Change in absorbance at 604 nm extracted from the rapid scanning experiments done in the presence of 25, 50, and 200 μM MV, respectively. The traces were fitted to a lag followed by an exponential increase, and the rate constants were 2.52, 3.48, and 2.2 s^{-1} for 25, 50, and 200 μM MV, respectively.

followed (Figure 9), there is a 300 ms lag, which corresponds to the time required for Clusters A, B, and C to be reduced, followed by an absorption increase due to MV reduction. As expected, the rate constant associated with the exponential phase (*V/K* for MV) is independent of MV concentration (2.52, 3.48, and 2.2 s^{-1} for 25, 50, and 200 μM, respectively). The initial slope depends on MV concentration, allowing estimation of the k_{cat}/K_m for MV to be 2.3 mM^{-1} s^{-1}. If the K_m for MV does not vary with the temperature, we would expect a k_{cat}/K_m of 4.5 mM^{-1} s^{-1} based on the k_{cat} of 5 s^{-1} at 10 °C and a K_m of 1.1 mM estimated at 25 °C (*5*), which is in good agreement with our data. Based on the k_{cat}/K_m for MV at 10 °C of 2.3 mM^{-1} s^{-1} and the k_{cat} of 5 s^{-1} at the same temperature, we can estimate a K_m for MV of 0.46 mM at 10 °C. This agrees well with the value calculated from the kinetic simulation (0.96 mM).

In summary, the stopped-flow and RFQ-EPR experiments demonstrate that pyruvate rapidly reduces Cluster A as it forms the HE-TPP radical intermediate. In the absence of CoA, the HE-TPP radical slowly decays as Cluster B is reduced. When CoA is present, radical decay (and Cluster B reduction) is accelerated by 10^5-fold.

Marcus and Eyring Analysis of the Electron-Transfer Reaction

The results described above pose several important questions. How does CoA cause a 10^5-fold increase in the rate of electron transfer from the HE-TPP radical to Cluster B? Are these the true electron-transfer reaction rates or do they correspond to another process that gates the electron-transfer reaction? Can the rate enhancement be related to ground-state destabilization, transition-state stabilization, or another phenomenon?

To determine if these are true electron-transfer reactions, we measured the temperature dependence of the rate of reduction of the two Clusters (B and C) in the presence and absence of CoA, and in the presence of desulfo-CoA. Then, the temperature dependencies of the electron-transfer rates were analyzed using eqs 3 and 4 (see Materials and Methods) from Marcus electron-transfer theory (*11*). We input the values of driving force ($\Delta G'^0$) for Cluster B (−25 mV) and Cluster C reduction (−125 mV) (*18*), and estimated the electronic coupling (H_{AB}) and reorganizational energy (λ) by fitting the observed rate constant of the electron-transfer reaction at different temperatures to eq 3. Then, the values of $\Delta G'^0$ and λ were included in eq 4 to calculate the β value and the edge-to-edge distance between the two redox centers, *r*. We also used a range of β values between 0.7 and 1.4 as fixed parameters in the fit (*13*). If the values obtained from the Marcus analysis are unreasonable [e.g., $H_{AB} > 80$ cm^{-1}, the threshold when solvent reorganization becomes rate-limiting (*19*)], the electron-transfer rate is considered to be gated by an adiabatic event. In that situation, the electron-transfer data were analyzed by the Eyring equation (eq 5).

Temperature Dependence of Cluster B Reduction in the Presence and Absence of CoA. In the presence of pyruvate and in the absence of CoA (Table 3 and Figure 6, Panel B, Trace B), the rates of Cluster B reduction and radical decay are very slow (0.001 s^{-1} at 10 °C). A single exponential decay equation fits the data well, and the derived rate constants can be plotted against temperature (panels A in Figures 10 and 11). By fitting these data to the Marcus equation (eq 3) (Figure 10, panel A), we obtain an electronic coupling constant, H_{AB}, of 0.07 cm^{-1}, which is well below the limited value of 80 cm^{-1}, indicating that Cluster B reduction is a true electron-transfer reaction (Table 2). The reorganizational energy (λ, 2.1 eV) also falls within the range of most true electron-transfer reactions, which are generally between 0.7 and 2.3 eV (*20*). The high λ value indicates that there is a large energy barrier for the electron-transfer reaction, which makes it a slow process. It is known that the electronic decay constant, β, in proteins varies between 0.7 and 1.4 $Å^{-1}$. The 1.4 $Å^{-1}$ value for β, which is at the limit for the protein-mediated electron coupling, would be consistent with the presence of water molecules in the electron-transfer pathway or significant through-space jumps (*21*). Although through-space jumps, when part of the electron-transfer pathway, are also associated with poor electronic coupling, they would not affect the reorganizational energy. On this basis, we consider the presence of water molecules as a major cause for the slow electron-transfer rate in the absence of CoA. The estimated electron-transfer distance from the fit varies between 14.6 and 19.3 Å (edge-to-edge), depending on the value of β. This electron-transfer distance is longer than the actual edge-to-edge distance between the HE-TPP radical and Cluster B (∼12 Å), which indicates that the electron-transfer pathway in the absence of CoA is not optimized.

When PFOR is reacted with pyruvate plus CoA, reduction of Cluster B (140 s^{-1} at 10 °C) occurs about 10^5-fold faster than in the absence of CoA. Due to the rapid electron-transfer rates, we could not follow the reaction at temperatures higher than 30 °C. Analyzing the temperature dependence of the electron-transfer rate according to Marcus theory yields an electronic coupling constant that is much higher than 80 cm^{-1} and a reorganizational energy that is well beyond the range of true electron-transfer reactions (Table 2 and Figure 10, panel C). The fit of these data with a H_{AB} constrained to 80 cm^{-1} (the limit for a true electron transfer) (Table 2, values in parentheses) is much worse than the unconstrained fit, which yields the H_{AB} value larger than the threshold (solid lines in Figure 10, panel C). Thus, unlike the slow reduction of Cluster B in the absence of CoA, which appears to be a

Table 2: Parameters Obtained from Fit of the Kinetic Data to the Marcus Equation and Eyring Equation

parameters	PFOR + pyruvate (Cluster B reduction)	PFOR + pyruvate + desulfo-CoA (Cluster B reduction)	PFOR + pyruvate + CoA (Cluster B reduction)	PFOR + pyruvate + CoA (Cluster C reduction)
ΔG^* (kJ/mol)[a]	88.47	97.3	56.84	64.3
ΔS^* [J/(mol·K)]	-144.3 ± 8.43	61.74 ± 21.43	20.43 ± 0.2	-14.54 ± 0.58
ΔH^* (kJ/mol)	45.45 ± 2.77	115.7 ± 7.17	62.94 ± 2.7	60.7 ± 175.7
H_{AB} (cm^{-1})	0.07 ± 0.035	73.7 ± 2.5	499.3 ± 4.8 (41.3 ± 0.8)	140.8 ± 1.13 (11.3 ± 0.3)
λ (eV)	2.1 ± 0.11	3.7 ± 0.007	2.6 ± 0.002 (2.1 ± 0.1)	2.6 ± 0.006 (2.1 ± 0.006)
β ($Å^{-1}$)	1.4	0.7	1(0.7)	1(0.7)
R (Å)	14.6 ± 0.017	7.3 ± 0.01	1.62 ± 0.0184 (8 ± 0.05)	4.2 ± 0.018 (11.7 ± 0.07)
$\Delta G^{0'}$ (J/mol)	-2423 ± 133	-2402 ± 377	-2409 ± 97.24	-12386 ± 102

[a] Calculated relative to the rate of the radical decay in the absence of coenzyme A.

Table 3: Energetics of Coenzyme A Binding and the Energetic Contribution of Different CoA Moieties to the Reaction

	K_D (mM)	k(25 °C) (s^{-1})	$\Delta\Delta G_{binding}$ (kJ/mol)	$\Delta\Delta G_{reaction}$ (kJ/mol)
pyruvate				
Cluster B	–	3.3×10^{-3}	–	–
Cluster C		3.3×10^{-3}		
coenzyme A				
Cluster B	0.002	690		−30.33
Cluster C	0.002	30		−22.6
desulfo-CoA				
Cluster B	0.033	5.3×10^{-4}	+6.94	+4.5
Cluster C	0.033	5.3×10^{-4}	+6.94	+4.5
dephospho-CoA				
Cluster B	0.29	163	+12.3	−26.7
Cluster C	0.29	30	+12.3	−22.6

	$\Delta\Delta G_{binding}$ (kJ/mol)	$\Delta\Delta G_{reaction}$ (kJ/mol)
thiol group		
Cluster B	−6.94	−34.5
Cluster C	−6.94	−26.7
3′-phospho group		
Cluster B	−12.1	−3.55
Cluster C	−12.1	0

true electron-transfer reaction, the rapid reduction observed in the presence of CoA appears to be gated by an adiabatic process. Fitting the temperature dependence of the electron-transfer rate to the Eyring equation (eq 5) (panels A and C, Figure 11) yields an activation energy of 64 kJ/mol. When the data were plotted according to the linearized form of the Eyring equation (Figure 11, panel B inset), there was no noticeable curvature, suggesting that the electron-transfer reaction in the presence of CoA is gated by a single process.

Effect of Desulfo-CoA on the Rate of Cluster B Reduction. When PFOR is reacted with pyruvate in the presence of desulfo-CoA, the rate of electron transfer from the HE-TPP radical to Cluster B is 10-fold *slower* than in the *absence* of CoA (Figure 12). The value of H_{AB} is close to the 80 cm^{-1} limit, and the reorganizational energy is well above the value expected for a true electron transfer (Table 2) (panel B in Figures 10 and 11), indicating a gated reaction. The lack of curvature when the data are plotted according to the linearized form of the Eyring equation (Figure 11, panel B inset) suggests that the electron-transfer reaction is gated by a single process. Since a single process appears to gate the reduction of Cluster B by the HE-TPP radical, whether CoA or desulfo-CoA are present, the gating mechanism might be the same, even though the rates differ by 10^5-fold.

Kinetic Isotope Effect on Cluster B Reduction. Many electron-transfer rates are gated by proton-transfer reactions. In this case, a solvent isotope effect might be observed. The rate of Cluster B reduction at 10 °C in the presence of pyruvate and CoA is 1.5-fold slower in D_2O than in H_2O (60 and 90 s^{-1}, respectively) (Figure 13). This is a relatively small solvent isotope effect, indicating that proton transfer is not a primarily rate-limiting step in this electron-transfer reaction. Thus, the gate is likely to be a phenomenon other than proton transfer.

Temperature Dependence of Cluster C Reduction. Based on Kinsim analysis, the rate constant for electron transfer from Cluster B to Cluster C (5 s^{-1} at 10 °C) seems to be independent of electron acceptor (MV). Since this rate equals the k_{cat} at 10 °C under saturating MV concentrations, we followed the temperature dependence of the k_{cat} at different CoA concentrations (Figure 14, panel A). Based on the Marcus analysis of the temperature dependence of this reaction, the reduction of Cluster C appears to be gated. The unsatisfactory fit assuming a true electron-transfer reaction is presented in Figure 14, panel B, with dashed lines. It is interesting that the activation free energy and enthalpy (Figure 14, panel C) are similar for the process that gates reduction of Clusters B and C. This supports the assignment of Cluster B reduction as a gated process.

Binding Energies and Catalysis

The electron-transfer rate enhancement conferred by CoA must originate from the effect of binding or chemistry. CoA is a large molecule, and, in the case of several CoA-dependent enzymes, the energy of binding CoA is translated into lowering the transition-state barrier for the reaction. This has been termed the Circe effect (*22*). To assess the binding energy contribution, we determined the K_D for CoA analogues that lack certain functionalities. By comparing the K_D value of these analogues with the K_D for CoA, we calculated the energetics of binding specific components of CoA. We focused also on the effect of these CoA analogues on the steady-state k_{cat} (Cluster C reduction) and on the rates of Cluster B reduction.

To determine the K_D for CoA, we measured the steady-state k_{cat} at saturating MV concentrations. Under these conditions, the steady-state k_{cat} equals the rate constant for Cluster C reduction. Furthermore, to address the possibility

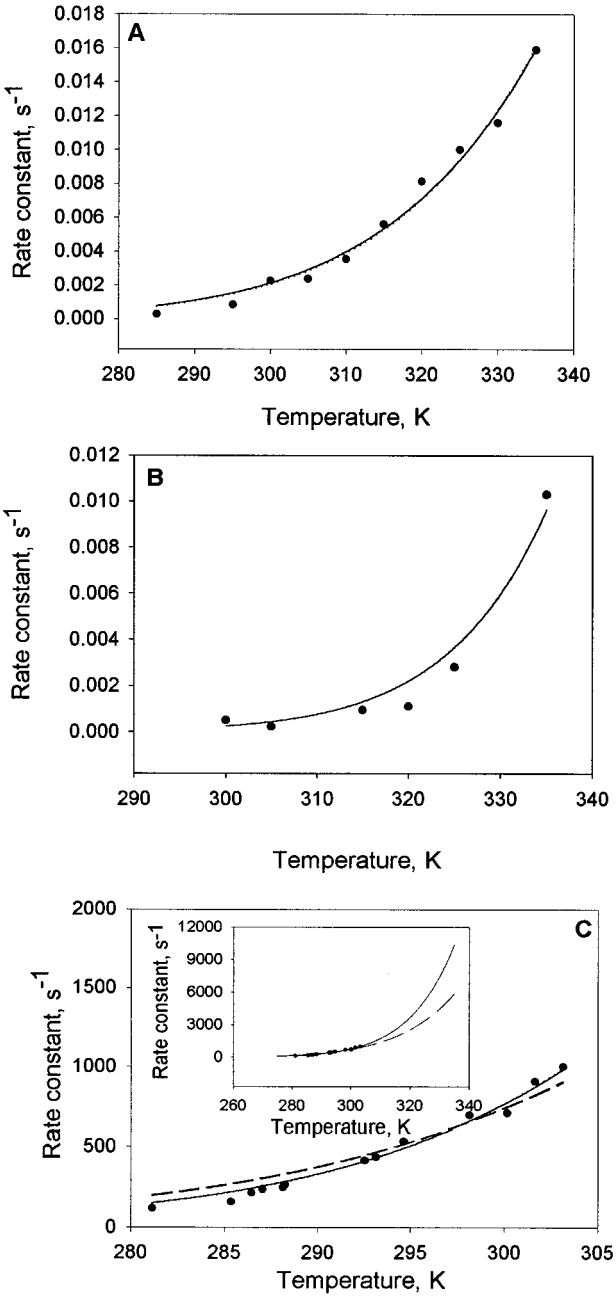

FIGURE 10: Temperature dependence of Cluster B reduction analyzed by Marcus theory. Panel A: PFOR plus pyruvate. Panel B: PFOR plus pyruvate in the presence of desulfo-CoA. Panel C: PFOR plus pyruvate in the presence of CoA. In panel C is plotted the temperature dependence of the fast phase rate constant. Dashed lines represent the fit with $H_{AB} < 80$ cm^{-1}. Inset: the extended plot (0−60 °C).

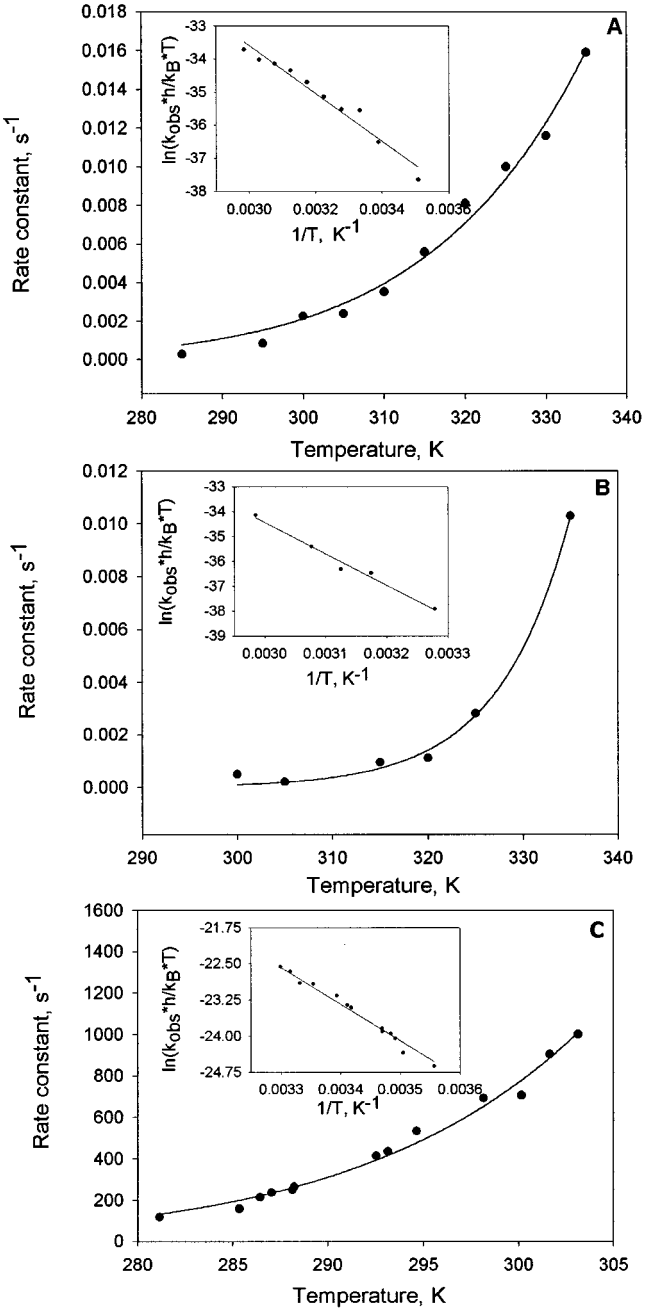

FIGURE 11: Temperature dependence of Cluster B reduction analyzed through Eyring transition-state theory. Panel A: PFOR plus pyruvate. Panel B: PFOR plus pyruvate in the presence of desulfo-CoA. Panel C: PFOR plus pyruvate in the presence of CoA. In panel C, we plotted the temperature dependence of the fast phase rate constant. Inset: The data were transformed and fitted to the linear form of the Eyring equation.

that binding of CoA is the gate that controls electron transfer from Cluster B to Cluster C, the temperature dependence of k_{cat} was determined. The K_M value for CoA is 2 μM and is temperature-independent (Figure 14, panel A). Given the strong temperature dependence of the electron-transfer reaction, this result suggests that CoA binding is not part of the gate that controls that rate of electron transfer. Desulfo-CoA was found to inhibit the steady-state reaction competitively with respect to CoA. The K_i value is 0.020 ± 0.006 mM (Table 3). Since the K_i(desulfo-CoA)/K_m(CoA) (K_i/K_d ratio) ratio is 9.75, the −SH group contributes −5.6 kJ/mol to the binding energy of CoA (Table 3).

To determine the effect of the thiol group on the rate of electron transfer from the HE-TPP radical to Cluster B, the rate of Cluster B reduction was measured in the presence (140 s^{-1}) and absence of CoA (0.001 s^{-1}) and in the presence of desulfo-CoA (10^{-4} s^{-1}). This reaction can be followed directly in the absence of external electron acceptor by measuring the bleaching of the 420 nm absorption feature. Comparing the electron-transfer rates in the presence and absence of CoA indicates that CoA lowers the activation barrier to this electron-transfer reaction by 30.6 kJ/mol. Strikingly, the rate of Cluster B reduction in the presence of desulfo-CoA is lower than that in the *absence* of CoA. By

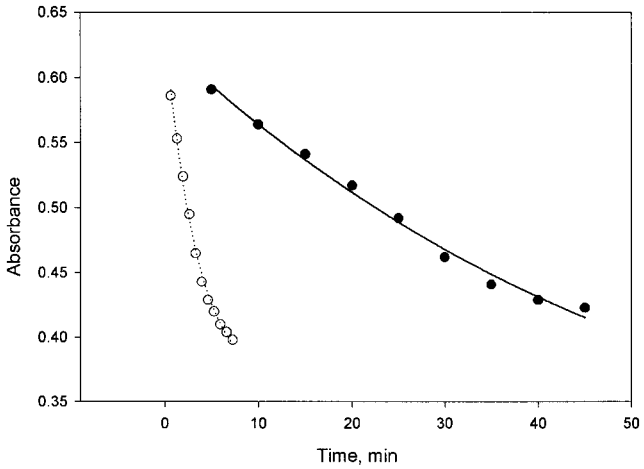

FIGURE 12: Spectral changes at 420 nm associated with Cluster B reduction in the presence of pyruvate (○) and pyruvate plus desulfo-CoA (●). Data represent Cluster B reduction at 40 °C. The solid and dotted lines represent the fit to the single exponential decay equation.

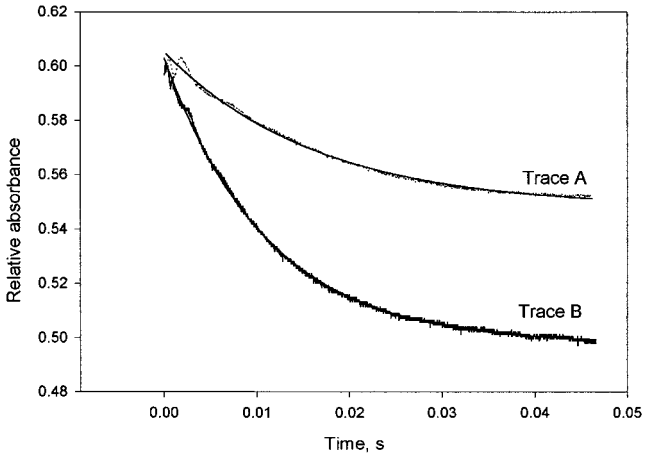

FIGURE 13: D_2O effect on Cluster B reduction. Trace A: the change in absorbance at 420 nm in the presence of D_2O ($A = 0.057$ OD, $k = 60.7$ s^{-1}). Trace B: the change in absorbance at 420 nm in the absence of D_2O ($A = 0.1$ OD, $k = 90.25$ s^{-1}). The differences in the amplitudes reflect the difference in enzyme concentration in the two experiments.

comparing electron-transfer rates in the presence of CoA versus desulfo-CoA, the −SH group can be calculated to lower the activation barrier for the electron-transfer reaction by 40.5 kJ/mol. Thus, the contribution of the thiol group to the electron-transfer rate is much (35 kJ/mol) greater than the modest 5.6 kJ/mol effect on binding energy (above). One caveat to this approach is that, since in the presence of CoA or desulfo-CoA the electron-transfer reaction is gated, the activation barrier under these conditions relates to the adiabatic process preceding electron transfer. This concept is considered more extensively under Discusion as the different mechanisms by which CoA controls the rate of electron transfer are examined.

PFOR uses 3′-dephospho-CoA as a relatively good substrate. From steady-state experiments following MV reduction, the K_m for dephospho-CoA is 0.21 ± 0.03 mM and the V_{max} is 8.6 ± 0.4 units/mg (Table 3). The V_{max} with pyruvate and CoA for this preparation of enzyme is 9 units/mg (18 s^{-1} at 25 °C). We repeated this experiment with another batch of enzyme (16 units/mg) and found the same K_m and a k_{cat} of 30 s^{-1} at 25 °C (5 s^{-1} at 10 °C); therefore, although the

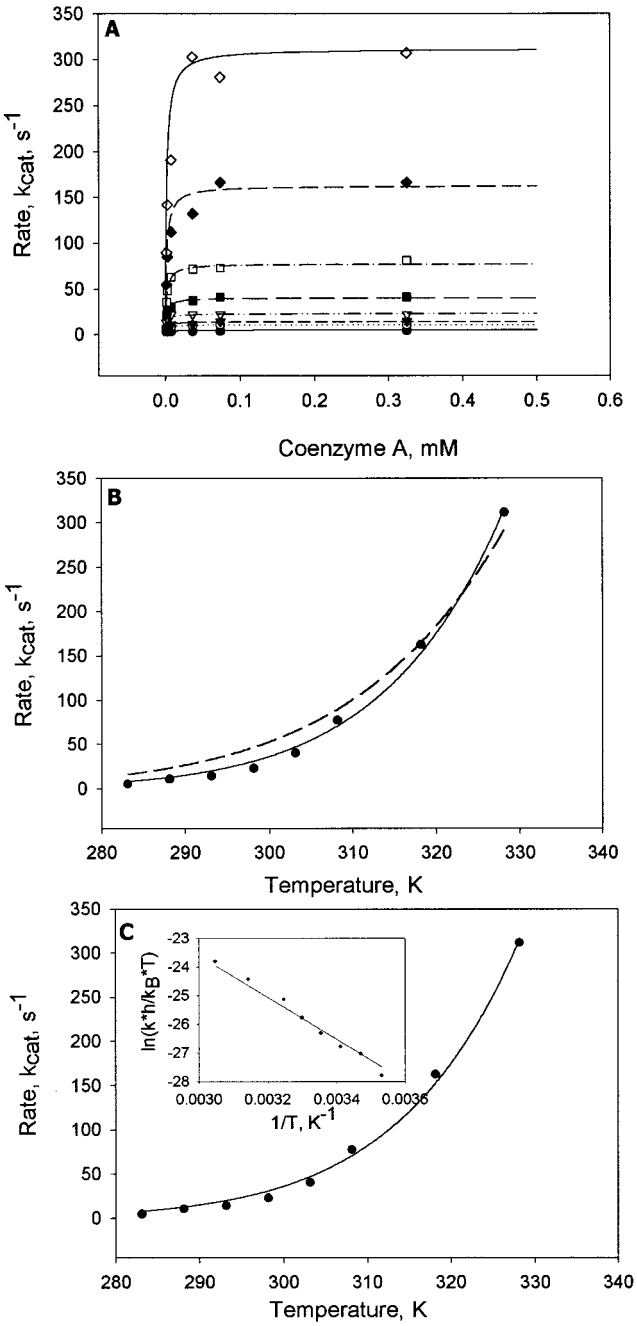

FIGURE 14: Temperature dependence of k_{cat}. Panel A: The dependence of the k_{cat} (which equals the rate of Cluster C reduction) on CoA concentration estimated at different temperatures (10−50 °C). At each temperature, the data were fitted to the Michaelis−Menten equation. Panel B: The k_{max} values obtained from the fit in panel A were plotted as a function of temperature and analyzed through electron-transfer theory. Dashed lines represent the fit with a $H_{AB} < 80$ cm^{-1}. The continuous line is the fit for gated electron transfer. Panel C: The data from panel B were analyzed by transition-state theory. Inset panel C: The data were transformed and fitted to the linear form of the Eyring equation.

K_m for 3′-dephospho-CoA is higher than that for CoA, the k_{cat} value is identical. We also followed the rates of Cluster B and Cluster C reduction in the presence of 3′-dephospho-CoA at 420 nm in a pre-steady-state experiment, and the stopped-flow data were fit to a double exponential equation. We relate these rates to Cluster A, Cluster B, and Cluster C reduction. The third rate constant, k_3, which depends strongly on the CoA concentration, is also the rate-limiting step for the overall reaction and is identical with the steady-state rate

of MV reduction. It was used to determine the K_D for 3′-dephospho-CoA and the k_{max} for the reaction. The first rate constant is higher (160 s^{-1} at 25 °C and saturating 3′-dephospho-CoA concentrations) and manifests a weaker dependence on 3′-dephospho-CoA concentration. The rate of Cluster B reduction is 160 s^{-1} at 25 °C, which is 4.3-fold smaller than with CoA (690 s^{-1} at 25 °C). The rate of Cluster C reduction was dependent on the 3′-dephospho-CoA concentration. Fitting the rate constant for Cluster C reduction to the Michaelis−Menten equation gave a k_{max} of 30.5 ± 0.6 s^{-1} and a K_D of 0.29 ± 0.02 mM (at 25 °C) which agrees with the steady-state K_m value (Table 3). For the 30 s^{-1} phase, 3′-dephospho-CoA has a 145-fold larger K_D than CoA, and the 3′-phospho group can be calculated to contribute 12.3 kJ/mol to the binding energy. On the other hand, the absence of this group has no apparent effect on the 30 s^{-1} electron-transfer rate (Table 3). Therefore, the phosphate group affects the electron-transfer pathway from the radical intermediate to Cluster B without influencing the pathway from Cluster B to Cluster C.

To summarize the results described above, one can dissect the contributions of different components of CoA to the binding energy. However, the effects of these groups on the rate of acetyl-CoA synthesis or on the electron-transfer rate from HE-TPP to the second cluster are unrelated to the binding energy effects. Clearly, this rate enhancement does not originate from the energy of CoA binding; therefore, a mechanism other than the Circe effect must be sought to explain this rate enhancement. A clue to the source of this rate enhancement is that the SH group itself lowers the activation barrier to electron transfer by 40 kJ/mol.

DISCUSSION

PFOR uses two cofactors, TPP and CoA, and three [4Fe-4S] clusters to catalyze the oxidative decarboxylation of pyruvate to form acetyl-CoA and CO_2. The C-2 center of the thiazolium ring of TPP forms an adduct with pyruvate that undergoes decarboxylation and subsequent one-electron transfer to generate a radical intermediate and a one-electron-reduced Fe-S cluster. Formation of the HE-TPP radical intermediate and the preceding steps each occur at a rate that is independent of CoA. The subsequent reactions are the focus of this paper. An electron is transferred from the HE-TPP radical to an Fe-S cluster at a rate that is enhanced by 10^5-fold by addition of CoA. Whether it occurs over a period of minutes (*minus* CoA) or milliseconds (*plus* CoA), oxidative decay of the radical is tightly coupled to Fe-S cluster reduction.

Since all three clusters absorb at the same wavelength, it is not an obvious assignment of which redox centers are involved in the various electron-transfer processes. We were able to isolate individual steps and assign their relevant intrinsic rate constants by varying mixing conditions (pyruvate alone, pyruvate plus CoA, etc.), by following reactions by different spectroscopic methods, and by global kinetic fitting and simulation methods. The rate constants in the overall 13-step mechanism shown in Step 1 are self-consistent. For example, the same value for k_2, associated with formation of the HE-TPP radical, fits the reaction between PFOR and pyruvate alone and the overall reaction between PFOR and pyruvate, CoA, and MV. We have attempted to extend this kinetic description to the physical picture offered by the crystal structure of four prosthetic groups separated by known distances (Figure 2). Therefore, the fastest electron-transfer rate corresponds to reduction of Cluster A (the proximal cluster), the 140 s^{-1} rate constant (10 °C) to reduction of Cluster B (the medial cluster), and the 5 s^{-1} rate constant (10 °C) to electron transfer from Cluster B to Cluster C (the distal cluster). This assignment is consistent with the studies of the partial reactions.

We consider five mechanisms by which CoA could facilitate this electron-transfer reaction. The first is that some of the binding energy associated with CoA binding is relegated into lowering the transition state for electron transfer. Incisive studies of how the binding energy of CoA is transformed into catalytic prowess (e.g., Jencks' Circe effect) in another CoA-dependent enzyme (*23*) prompted us to speculate that binding of CoA to PFOR might drive this 10^5-fold rate enhancement. However, this hypothesis is inconsistent with comparisons between the effects of various components of CoA on the binding energy and their effects on the electron-transfer rate and on catalysis. The most striking negation of this hypothesis is that the sulfur atom of CoA contributes only 5.6 kJ/mol to the binding energy, whereas it lowers this activation barrier for electron transfer by a remarkable 40 kJ/mol. Thus, the sulfur atom is the major contributor to the rate enhancement. Furthermore, when PFOR reacts with desulfo-CoA, which contains all of the binding determinants present on CoA except the sulfur, the rate of electron transfer is 10-fold slower than in the absence of CoA. Therefore, binding interactions between PFOR and CoA could play only a minor role and certainly are not responsible for a 10^5-fold rate enhancement for reduction of Cluster B by the HE-TPP radical intermediate.

The next four hypothetical mechanisms by which CoA elicits this 10^5-fold rate enhancement are evaluated using Marcus theory and Eyring theory. This analysis also is subject to the assumptions we have made in relating the kinetically assigned cluster to the structural assignments (described above). Marcus analysis of the electron-transfer rates demonstrates that Cluster B reduction by the HE-TPP radical in the presence of CoA exhibits an H_{AB} value beyond the range for reactions in which electron transfer is rate limiting. Thus, an adiabatic process appears to gate this reaction. Surprisingly, it apparently becomes ungated, i.e., a true electron-transfer reaction, in the absence of any CoA analogues, where the rate constant is 0.18 min^{-1}. Therefore, CoA introduction is associated with a gating of the electron transfer; however, instead of decreasing the electron-transfer rate, the gating phenomenon is associated with a marked rate enhancement. Similarly, ATP gates electron transfer from the Fe protein to the MoFe protein in nitrogenase while accelerating the rate above that of true electron transfer (*24*). The gated reaction is also faster than the true electron transfer in methylamine dehydrogenase (*25*). Since desulfo-CoA also generates a gated electron-transfer reaction, we assume that the dominant effect of the sulfur of CoA on electron transfer is not a component of this gate. In other words, the sulfur atom of CoA is predominantly responsible for the 10^5-fold rate enhancement, but this effect is dampened by some other component of the CoA structure. To evaluate the four mechanisms described below, we used Marcus theory (eq 4) to estimate the changes in $\Delta G^{0'}$, λ, β, and r that would be

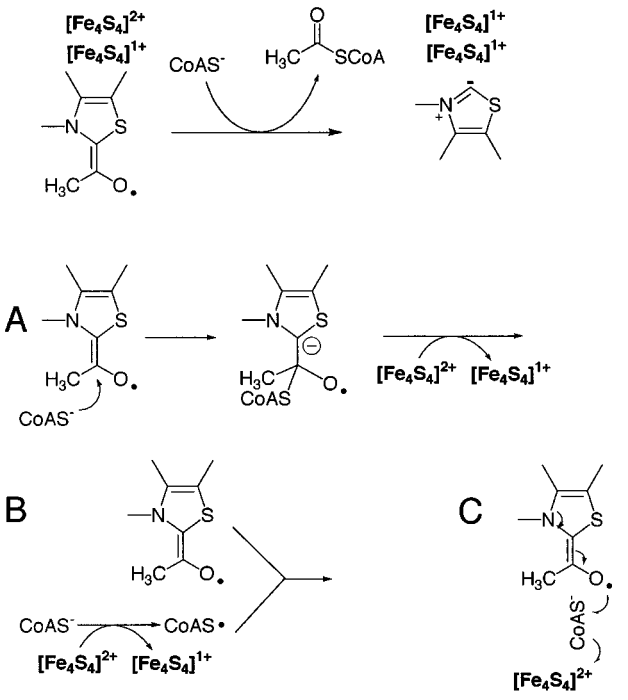

FIGURE 15: Radical decay possibilities. (A) Kinetic Coupling Mechanism: nucleophilic attack by the CoA thiolate on the HE-TPP radical generates a very reducing anion radical with a strong driving force for electron transfer to Cluster B. (B) Biradical Mechanism: Electron transfer from CoA to Cluster B generates a thiyl radical that combines with the HE-TPP radical. (C) Wire Mechanism: CoA induces the formation of an effective through-bonded electron-transfer pathway that connects the HE-TPP radical to Cluster B.

required to explain a 10^5-fold increase in the rate of Cluster B reduction. Since these rates characterize gated electron-transfer reactions, they set the lower limit of the true electron-transfer rate; the real electron-transfer rates are probably higher than these values. Thus, the activation barrier for the reduction of cluster B in the presence of CoA or desulfo-CoA relates to an adiabatic step preceding electron transfer, i.e., a different rate-determining step.

The second mechanism to consider as an explanation for the electron-transfer rate enhancement is that binding of CoA induces a conformational change in PFOR that brings the electron donor (HE-TPP radical) and acceptor (Cluster B) closer together. To assess this *Conformational Change Mechanism*, we fixed the reorganization energy at 2.1 eV and the $\Delta G^{0'}$ at -0.025 eV (HE-TPP radical $-$ Cluster B). Then, we calculate that achievement of a 10^5-fold increase in electron-transfer rate requires the distance between the donor and acceptor centers to shorten by 8.25 Å (from 14.5 to 6.25 Å) or the electronic decay constant to become 0.4 $Å^{-1}$. We look forward to solution of the crystal structure of the PFOR−CoA complex, which should directly negate or support this hypothetical mechanism. We suggest that a conformational change is not a likely solution to the problem because binding of desulfo-CoA and CoA should induce similar structural changes. Yet the rate of electron transfer differs by 10^6-fold different between these analogues.

We do not feel that we can offer overwhelming support for or evidence against the three remaining mechanisms that will be described (Figure 15). Furthermore, these mechanisms are not mutually exclusive. In Mechanism A, the *Kinetic Coupling Mechanism*, nucleophilic attack by the CoA thiolate on the HE-TPP radical generates a very reducing anion radical that would have a much higher driving force for electron transfer to Cluster B. Note that the chemical coupling could not occur with desulfo-CoA, since it cannot generate the radical adduct. In this mechanism, a chemical step (formation of the covalent adduct with the radical) would be tightly coupled to (and could be rate limiting for) the electron-transfer reaction. In this mechanism, CoA may not significantly change the r, β, or the reorganizational energy λ, but would have a major effect on the driving force. According to this scenario (fixing r, β, and λ), to achieve the 10^5-fold increase in this electron-transfer rate, we calculate that a 630 mV difference between the redox potentials of the radical (or anion radical) intermediate and Cluster B must be attributed to the thiol of CoA. This does not seem too unreasonable since an anion radical would be a strongly reducing species and this radical intermediate would only need to be stable enough for the rapid electron-transfer reaction ($\sim$5 ms). This is an attractive proposal, and chemical models of such a species and theoretical modeling of such a reaction intermediate would be extremely helpful.

Besides the driving force, we also would expect a change in the reorganizational energy, if the HE-TPP radical is converted to a thiyl anion radical intermediate. Assuming an increase in the negative charge on the proposed radical anion intermediate, water molecules and/or positive charges on the neighboring amino acids would be expected to rearrange to compensate for the extra negative charge, which would increase the reorganizational energy. If we assume that only the reorganization energy is altered (i.e., the presence of CoA does not change the r, β, and the free energy $\Delta G'^0$), the λ must be lowered from 2.1 to 0.97 eV to attain the 10^5-fold rate enhancement. This is an unlikely scenario since the reorganizational energy associated with cluster reduction is expected to be about 1.6 eV (*26*), leaving only 0.5 eV to be associated with the radical/thiyl radical intermediate. However, binding of CoA would decrease the reorganizational energy by excluding the water from the active site of the enzyme, which should compensate. Thus, changes in reorganization energy and driving force may both contribute to the overall rate enhancement. For example, a change in reorganizational energy of 0.5 eV (from 2.1 to 1.6 eV) and a 120 mV more negative redox potential of the radical or radical anion intermediate (increasing the driving force) will result in a 10^5-fold increase in the electron-transfer rate. We wish to reemphasize that biomimetic models and theoretical studies are necessary to evaluate the feasibility of this mechanism. Although it is clear that the radical anion intermediate proposed in the Chemical Coupling Mechanism would be a stronger reductant than the HE-TPP radical, however, we are unaware of any chemical models of such a species or a pair of analogous radicals for comparison.

Mechanism B, the *Biradical Mechanism*, involves electron transfer from CoA to Cluster B to generate a thiyl radical that combines with the HE-TPP radical. Without the sulfur atom, it would be impossible to form a radical species analogous to the thiyl radical of CoA. A merit of the biradical mechanism is that it would be spin-favored, whereas reaction between a radical and a nucleophile is spin-forbidden. Reduction of one Fe-S cluster has been observed when PFOR is reacted with CoA alone, which supports the biradical

mechanism (*5*). However, the putative sulfur-based radical has not been observed in such reactions. A CoA thiyl radical has been detected in hydrogenosomes from *Tritrichomonas foetus* (*27*). Model studies on the TPP analogues reveal the ease with which HE-TPP radicals recombine in solution (*28*).

In Mechanism C, the *Wire Mechanism*, CoA induces the formation of an effective through-bonded electron-transfer pathway that connects the electron donor, the HE-TPP radical, to the electron acceptor. According to this mechanism, the electron-transfer pathway in the absence of CoA is inefficient. Electron transfer through covalent bonds is more favorable than through solvent or through space (*19*). Possibly, CoA binding induces the formation of a new and favored covalently bonded pathway for electron transfer between the HE-TPP radical and Cluster B. In the transition state for thioester formation, the CoA thiol group must be in van der Waals contact with carbon-1 of the hydroxyethyl moiety. CoA itself could serve as a ~20 Å long wire that connects the radical intermediate to Cluster B. Thus, the economy (parsimony) of Nature could provide two necessary, but seemingly disparate, functions to CoA. One is to form the chemical linkage required for further metabolism of the acetyl group; the other is to bridge two redox centers, which accelerates completion of the first half-reaction in the PFOR mechanism. This could be accomplished by a CoA-induced conformational change. However, a conformational change might not be required. Perhaps CoA itself could be a component of this electron-transfer pathway. In this scenario, one might think of CoA as a wire and the thiol group as the prong that connects to the electron source at the socket. The requirement of the sulfur atom of CoA in such a mechanism would be analogous to plugging a wire into an outlet; without the thiol group, there would be a significant gap between the electron donor and the CoA that slows electron transfer by 10^5-fold. However, it appears unlikely that this would be the exclusive mechanism of rate enhancement. First, if CoA were simply bridging the pathway, the resulting electron transfer would not be gated, but would be a true electron transfer with an increased coupling. Second, assuming that they bind in the same manner (which is probably true since the K_d values of CoA and desulfo-CoA are similar), most of the covalent electron-transfer pathway should be present in desulfo-CoA, which makes electron transfer 10^6-fold slower than with CoA. The penalty associated with a gap between the radical and the methyl carbon (at the beginning of the wire) would not be expected to approach such a value.

It is possible that Mechanisms A, B, and C could all contribute to the overall 10^5-fold rate enhancement. Furthermore, CoA binding could contribute in other ways to rate enhancement. For example, CoA binding might be accompanied by the exclusion of water molecules between the two redox active centers and/or solvent reorganization around the redox centers. These structural changes would decrease both the electronic decay constant and the reorganization energy, which would facilitate a faster electron transfer. This mechanism could be ruled out or supported by the crystal structure of the PFOR−CoA complex; however, this is not yet available. One can estimate the maximum number of water molecules that could be excluded upon CoA binding if water exclusion is solely responsible for the increase in the ET rate through the mechanisms described above. For adiabatic reactions, such as the process that gates the electron transfer from the radical intermediate to Cluster B, the Eyring equation is most appropriate. Treatment of the data by the Eyring equation reveals that when CoA is present, the ΔG_{cat} for the process that gates the electron-transfer reaction is 56.84 kJ/mol (at 25 °C). Binding of CoA results in a 32 kJ/mol lowering of a high entropic barrier; i.e., the rate enhancement is mostly entropic. Binding of CoA could decrease the entropy barrier by the hydrophobic effect. It has been estimated that the free energy associated with the burial of hydrophobic groups is about 100.4 J/(mol·Å^2) (*29*, *30*). If the 32 kJ/mol originates from water exclusion, 300 Å^2 of protein surface shifts from interactions with the solvent to hydrophobic interactions with CoA and/or other protein residues. Considering 10 Å^2/H_2O molecule (*31*), about 30 molecules of water would be released from the active site when CoA binds to the protein. Release of these waters would promote a more compact structure, a lower reorganizational energy, which could enhance the electron-transfer reaction.

REFERENCES

1. Yoon, K. S., Hille, R., Hemann, C., and Tabita, F. R. (1999) *J. Biol. Chem. 274*, 29772−29778.
2. Yoon, K. S., Ishii, M., Kodama, T., and Igarashi, Y. (1997) *Arch. Microbiol. 167*, 275−279.
3. Furdui, C., and Ragsdale, S. W. (2000) *J. Biol. Chem. 275*, 28494−28499.
4. Chabriere, E., Charon, M.-H., Volbeda, A., Pieulle, L., Hatchikian, E. C., and Fontecilla-Camps, J.-C. (1999) *Nat. Struct. Biol. 6*, 182−190.
5. Menon, S., and Ragsdale, S. W. (1997) *Biochemistry 36*, 8484−8494.
6. Chabriere, E., Vernede, X., Guigliarelli, B., Charon, M. H., Hatchikian, E. C., and Fontecilla-Camps, J. C. (2001) *Science 294*, 2559−2563.
7. Andreesen, J. R., Schaupp, A., Neurater, C., Brown, A., and Ljungdahl, L. G. (1973) *J. Bacteriol. 114*, 743−751.
8. Menon, S., and Ragsdale, S. W. (1996) *Biochemistry 35*, 12119−12125.
9. Elliott, J. I., and Brewer, J. M. (1978) *Arch. Biochem. Biophys. 190*, 351−357.
10. Gray, H. B., and Malmstrom, B. G. (1989) *Biochemistry 28*, 7499−7505.
11. Marcus, R. A., and Sutin, N. (1985) *Biochim. Biophys. Acta 811*, 265−322.
12. Davidson, V. L. (2000) *Acc. Chem. Res. 33*, 87−93.
13. Davidson, V. L. (2000) *Biochemistry 39*, 4924−4928.
14. Zimmerie, C. T., and Frieden, C. (1989) *Biochem. J. 258*, 381−387.
15. Barshop, B. A., Wrenn, R. F., and Frieden, C. (1983) *Anal. Biochem. 133*, 134−145.
16. Guo, F. S., Zhang, D. Q., Kahyaoglu, A., Farid, R. S., and Jordan, F. (1998) *Biochemistry 37*, 13379−13391.
17. Wahl, R. C., and Orme-Johnson, W. H. (1987) *J. Biol. Chem. 262*, 10489−10496.
18. Pieulle, L., Guigliarelli, B., Asso, M., Dole, F., Bernadac, A., and Hatchikian, E. C. (1995) *Biochim. Biophys. Acta−Protein Struct. Mol. Enzymol. 1250*, 49−59.
19. Gray, H. B., and Winkler, J. R. (1996) *Annu. Rev. Biochem. 65*, 537−561.
20. Lee, H. J., Basran, J., and Scrutton, N. S. (1998) *Biochemistry 37*, 15513−15522.
21. Ponce, A., Gray, H. B., and Winkler, J. R. (2000) *J. Am. Chem. Soc. 122*, 8187−8191.
22. Jencks, W. P. (1975) *Adv. Enzymol. Relat. Areas Mol. Biol. 43*, 218−409.
23. Whitty, A., Fierke, C. A., and Jencks, W. P. (1995) *Biochemistry 34*, 11678−11689.
24. Lanzilotta, W. N., Parker, V. D., and Seefeldt, L. C. (1998) *Biochemistry 37*, 399−407.
25. Hyun, Y.-L., Zhu, Z., and Davidson, V. L. (1999) *J. Biol. Chem. 274*, 29081−29086.

26. Sigfridsson, E., Olsson, M. H. M., and Ryde, U. (2001) *Inorg. Chem. 40*, 2509−2519.
27. Docampo, R., Moreno, S., and Mason, R. (1987) *J. Biol. Chem. 262*, 12417−12420.
28. Barletta, G., Chung, A. C., Rios, C. B., Jordan, F., and Schlegel, J. M. (1990) *J. Am. Chem. Soc. 112*, 8144−8149.
29. Chlothia, C. (1974) *Nature 248*, 338−339.
30. Dill, K. A. (1990) *Biochemistry 29*, 7133−7155.
31. Weber, G. (1993) *J. Phys. Chem. 97*, 7108.

BI0257641